

Article

Robust Control of Frequency Variations for a Multi-Area Power System in Smart Grid Using a Newly Wild Horse Optimized Combination of PIDD² and PD Controllers

Mohammed Khudhair ¹, Muhammad Ragab ² , Kareem M. AboRas ^{2,*}  and Nabil H. Abbasy ²¹ Iraqi Ministry of Defense, Baghdad 10011, Iraq; mm5679607@gmail.com² Department of Electrical Power and Machine Engineering, Faculty of Engineering, Alexandria University, Alexandria 21544, Egypt; muhammadragab2020@gmail.com (M.R.); nabil.abbasai@alexu.edu.eg (N.H.A.)

* Correspondence: kareem.aboras@alexu.edu.eg

Abstract: This paper proposes a new combined controller, the proportional integral derivative-second derivative with a proportional derivative (PIDD²-PD), to improve the frequency response of a multi-area interconnected power system with multiple generating units linked to it. The optimum gains of the presented controller are well-tuned using a wild horse optimizer (WHO), a modern metaheuristic optimization approach. The main study is a two-area-linked power system with varied conventional and renewable generating units. The physical constraints of the speed turbines and governors are considered. The WHO optimization algorithm is proven to outperform various other optimization approaches, such as the whale optimization algorithms (WOA) and chimp optimization algorithms (ChOA). The efficacy of the proposed WHO-based PIDD²-PD controller is evaluated by comparing its performance to other controllers in the literature (cascaded proportional integral derivative-tilted integral derivative (PID-TID), integral derivative-tilted (ID-T) controller). Multiple and varied scenarios are applied in this work to test the proposed controller's sturdiness to various load perturbations (step, random, and multi-step), renewable energy source penetration, and system parameter variations. The results are provided as time-domain simulations run using MATLAB/SIMULINK. The simulation results reveal that the suggested controller outperforms other structural controllers in the dynamic response of the system in terms of settling time, maximum overshoot, and undershoot values, with an improvement percentage of 70%, 73%, and 67%, respectively.

Keywords: combined PIDD²-PD proportional integral derivative-second derivative-proportional-derivative controller; wild horse optimizer; multi-source power system; renewable sources; load frequency control; two-area system



Citation: Khudhair, M.; Ragab, M.; AboRas, K.M.; Abbasy, N.H. Robust Control of Frequency Variations for a Multi-Area Power System in Smart Grid Using a Newly Wild Horse Optimized Combination of PIDD² and PD Controllers. *Sustainability* **2022**, *14*, 8223. <https://doi.org/10.3390/su14138223>

Academic Editor: Thanikanti Sudhakar Babu

Received: 5 May 2022

Accepted: 30 June 2022

Published: 5 July 2022

Publisher's Note: MDPI stays neutral with regard to jurisdictional claims in published maps and institutional affiliations.



Copyright: © 2022 by the authors. Licensee MDPI, Basel, Switzerland. This article is an open access article distributed under the terms and conditions of the Creative Commons Attribution (CC BY) license (<https://creativecommons.org/licenses/by/4.0/>).

1. Introduction

Recent power systems have turned out to be more complicated because of the loads' multiplicity and the renewable energy sources (RESs)' penetration to mitigate the drawbacks of traditional power sources. The rate of penetration of RESs, such as wind and solar plants, into newly established power systems is deemed to be economically beneficial and positive because it reduces the consumption of the oil, coal, and gas used to operate traditional power plants, whereas the combustion of oil and coal results in the release of carbon dioxide gas, which exacerbates the ozone hole and the global warming phenomenon. Although the existence of RESs in electrical power networks cheapens the operating costs and lessens the severity of pollution caused by conventional units, these renewable sources lack system inertia, which affects system stability, and increases frequency deviations [1,2]. As a result, in addition to the challenges posed by mismatching between demand and generation, modern power systems are exposed to new challenges because of RESs integration. These challenges have an impact on the power grid's stability and security [3]. As a result, load frequency control (LFC) is regarded as an important key for keeping system

frequency under control and managing the tie-lines power transfer between the areas of the power system.

1.1. Literature Review

For numerous power system architectures, the problem of frequency stability has been addressed. Researchers in [4,5] investigated LFC for one-area systems, whereas [6–8] investigated a multi-area system with nonlinearities, while [9,10] examined a deregulated power system. Several control methods have been used to solve the problem of load frequency control in power systems. These include model predictive control (MPC) [11], artificial intelligence control [12], robust control approaches [13], and fuzzy logic control [14,15]. Due to its simplicity and cheapness, academic researchers have concentrated their studies on the conventional PID controller. Despite this, the PID controller has a tough time adjusting its settings by trial and error in the face of system nonlinearities and disturbances. As a result, research effort has been expended in determining the best PID controller parameters. In this aspect, the appropriate PID design methodology stemming from different optimization techniques has been applied to the load frequency control (LFC) problem [16,17]. Fractional-order (FO) controller structures, on the other hand, have been quickly expanding due to their flexibility and wider degree of freedom. The fractional-order calculus (FOC) category also includes a tilted integral derivative (TID) controller structure, which has been employed to overcome load frequency control difficulties. The benefits of a TID controller are that it is easier to tune, has a higher disturbance rejection ratio, and has fewer plant effects. Consequently, the TID controller was introduced as an alternative to the LFC issues in various research works [18–20]. In addition, refs. [21,22] offers a composite controller based on integrating TID and fractional-order proportional derivative (FOPID) controllers to receive the benefits of both. It has simpler tuning, a better disturbance rejection ratio, and fewer effects on the plant.

The cascaded controller structure has lately been employed instead of the traditional controller structure due to its efficacy and superior performance. As a result, many types of cascaded controllers have been deployed to enhance frequency stability in power systems [9,23–25]. In load frequency control research, another way was investigated recently, which is focused on combining two controllers [26,27].

In addition, authors in [28] proposed an integral-proportional derivative I-PD controller structure to minimize the frequency variations in a two-area interconnected power system. The performance of the I-PD controller outperforms that of the PID controller. In addition, for the load frequency control, refs. [29,30] proposed the integral-tilt derivative (I-TD) controller. The ID-T controller provided in [31] outperforms the TID controller in terms of system frequency performance. However, the proposed PIDD²-PD surpasses both the ID-T and PID-TID controllers in [31,32], respectively. According to prior research, picking the controller settings is just as important as choosing the controller type. The frequency stability issue has benefited greatly from the evolutionary optimization methodologies used to improve the controller parameters. As a consequence, choosing an appropriate optimization technique in the design procedure of the controller is a basic and crucial challenge. Classical optimization procedures were previously utilized to find the best frequency controller settings [18,33]. Additionally, ref. [34] presents a fuzzy gain scheduling (FGS) controller for parameter selection. These algorithms, however, face several difficulties, including slumps, deathtraps in local minimums, the demand for several iterations, and reliance on initial conditions for selecting the optimal settings. As a result, scholars overcame these obstacles by improving meta-heuristic optimization methods, such as the grey wolf optimizer [33], particle swarm optimization [35], ant lion optimization [36], chimp optimization algorithm [5], teaching-learning-based optimization [37], moth-flame optimization [11], equilibrium optimization [38], and atom search optimization [39]. Substantial emphasis has been placed on the use of various optimization techniques to assist them in tackling technical difficulties, particularly the load frequency control issue. Therefore, the author chose to use the wild horse optimizer (WHO) [40] in this work to identify the best settings for the proposed PIDD²-PD controller. The primary result from prior research is that LFC

techniques that depend on the controller designer's talents, such as fuzzy logic control, H-infinite approaches, and MPC, meet the needed performance requirements but have many design problems and take considerable time to choose the control settings. Additionally, traditional PD, PI, and PID controllers struggle to cope with system uncertainties. Numerous previous articles paid insufficient attention to robustness evaluations, such as system nonlinearities and system parameter variations. Additionally, most previous assessments failed to account for considerable renewable energy integration in the absence of system parameter changes by including system uncertainties, nonlinearities, and simultaneous load variations.

1.2. Contribution of Paper

This study proposes a novel combination PIDD²-PD controller that improves system frequency stability considering renewable power perturbations. Additionally, the suggested PIDD²-PD controller's settings have been developed in line with the WHO to preserve both frequency and system stability under abnormal situations. In contrast to other research on related issues, the following is a summary of the paper's key contribution:

- Using a reliable PIDD²-PD controller to enhance the frequency stability of a two-area interconnected power system considering RESs;
- Using the WHO algorithm to optimize the parameters of the presented PIDD²-PD controller, a novel and effective optimization approach for LFC design;
- Demonstrating the WHO's superiority by comparisons to the performance of more complex algorithms (e.g., the chimp optimization algorithm (ChOA) [41] and the whale optimization algorithm (WOA) [42]);
- Validating the presented PIDD²-PD controller's efficacy by comparing it to the performance of various control strategies described in the literature (e.g., ID-T controller and PID-TID in [31,32], respectively);
- Testing the effectiveness and stability of the proposed controller when the studied two-area interconnected power system is subjected to various disturbances, such as different step load disturbances (SLD), multi-step load disturbances (MSLD), random load disturbances (RLD), RESs fluctuations, and communication time delay.

The remaining of the work is organized in the following manner: Section 2 details the architecture of the investigated system, describing each component. Section 3 introduces the suggested WHO algorithm, while Section 4 details the designed controller configuration. Section 5 summarizes the outcomes of several situations and discusses them. Finally, Section 6 contains the conclusion.

2. The Proposed Power System Modeling

The system under discussion is a connected hybrid power system with two areas. Each area has three dynamic subsystems: a reheat-turbine thermal power plant, a hydraulic power plant, and a gas unit, as illustrated in Figure 1. The system's nonlinearity is considered in terms of the physical limits of the power system, such as the GDB and GRC. Additionally, RESs are included (PV unit in the first area and a wind unit in the second area), as shown in Figure 2. The nominal load for each area is 1740 MW, and the rated power is 2000 MW. Details and system parameters for the system under study can be found in [21,43].

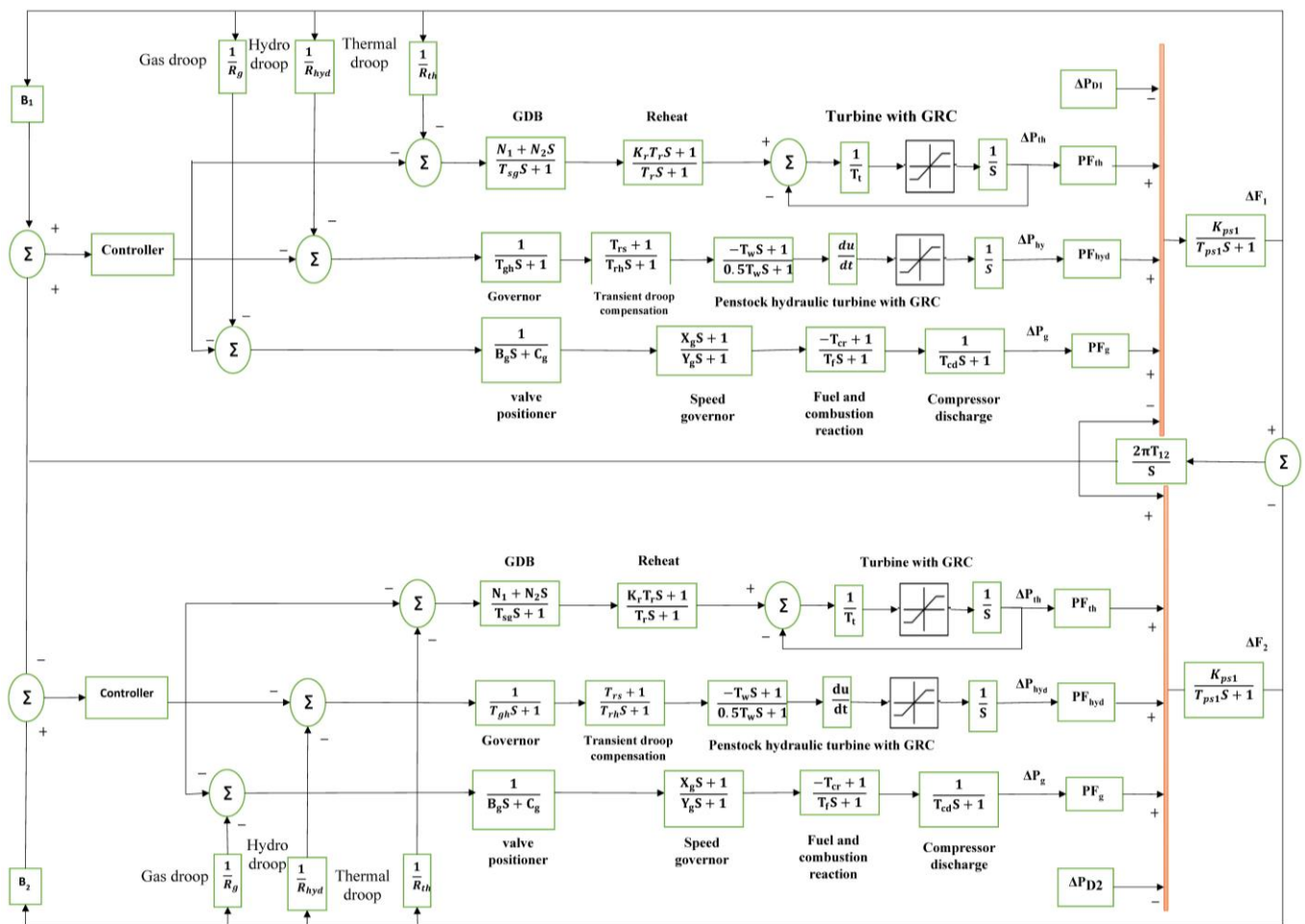


Figure 1. The dynamic model consists of a two-area power system with multiple sources.

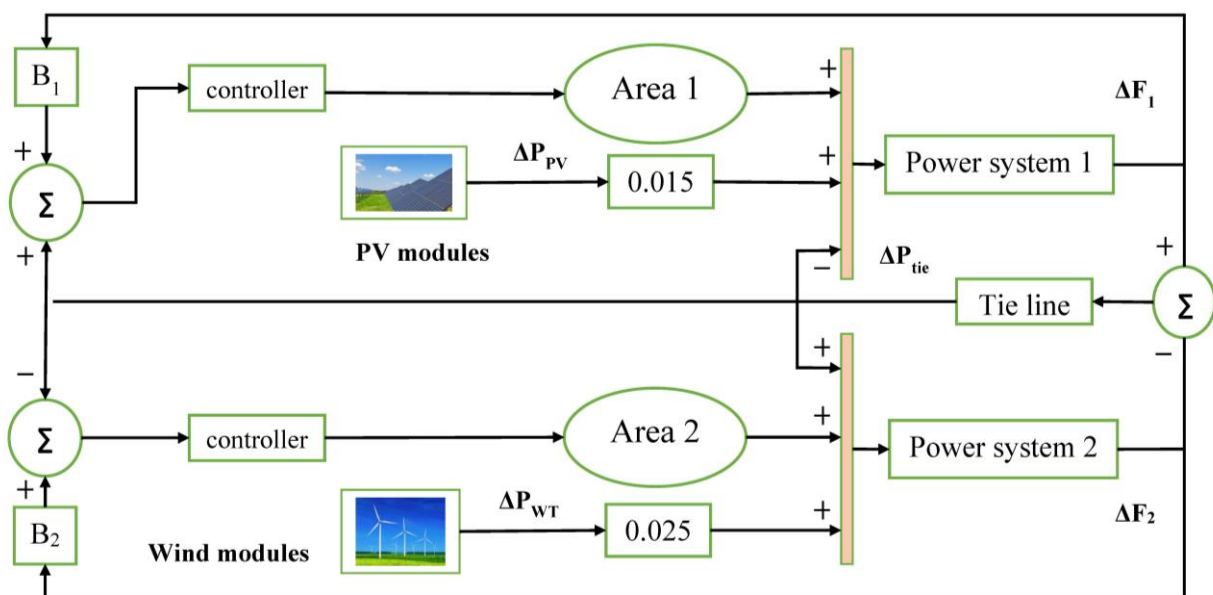


Figure 2. The system model with RESs.

2.1. Models of Dynamic Subsystems

2.1.1. Thermal Power Plant Supplies 1000 MW and Includes

- Governor dead band (GDB): The GDB non-linearity formulas could be simplified as a function of changes and change rates in speeds [21]. With the aid of the Fourier series, the transfer function of a GDB with 0.5% backlash is derived as:

$$\text{GDB} = \frac{N_1 + N_2 \cdot s}{T_{sg} \cdot s + 1} \quad (1)$$

In which the Fourier coefficients of $N_1 = 0.8$ and $N_2 = -0.2/\pi$ [19], and the time constant of the steam turbine T_{sg} is 0.06 s.

- Reheat is modeled using the first-order transfer function:

$$\text{Reheat} = \frac{k_r T_r \cdot s + 1}{T_r \cdot s + 1} \quad (2)$$

with a steam turbine reheating constant K_r of 0.3 and a steam turbine reheating time constant T_r of 10.2 s.

- Turbine with GRC

The generation rate constraint (GRC) for the thermal unit is set at 10% p.u./min (0.0017 p.u. MW/s). For rising and decreasing rates and a steam turbine time constant T_t of 0.3 s.

2.1.2. Hydraulic Power Plant Supplies 500 MW and Includes

- A Governor is modeled using the first-order transfer function, with a time constant for a hydro turbine governor $T_{gh} = 0.2$ s.

$$\text{Governor} = \frac{1}{T_{gh} \cdot s + 1} \quad (3)$$

- Transient droop compensation is modeled using a first-order transfer function, with hydro turbine speed governor reset time T_{rs} and a time constant of transient droop T_{rh} of 4.9 and 28.749 s, respectively.

$$\text{TDC} = \frac{T_{rs} \cdot s + 1}{T_{rh} \cdot s + 1} \quad (4)$$

- Penstock hydraulic turbine with GRC

The Penstock hydraulic turbine is modeled using the first-order transfer function with a starting time of water in hydro turbine $T_w = 1.1$ s.

$$\text{Penstock} = \frac{-T_w \cdot s + 1}{0.5T_w \cdot s + 1} \quad (5)$$

The GRC of the hydropower station is 270% p.u./min = (0.045 p.u. MW/s) and 360% p.u./min = (0.06 p.u. MW/s), respectively, for both rising and decreasing rates.

2.1.3. Gas Power Station Supplies 240 MW and Includes

- The valve positioner is modeled using the first-order transfer function with a time constant of the valve positioner B_g and the gas turbine valve positioner C_g of 0.049 and 1 s, respectively.

$$\text{Valve positioner} = \frac{1}{B_g \cdot s + C_g} \quad (6)$$

- The speed governor is modeled using the first-order transfer function with lead and a lag time constant of the gas turbine governor X_g , Y_g of 0.6 and 1.1 s, respectively.

$$\text{speed governor} = \frac{X_g \cdot s + 1}{Y_g \cdot s + 1} \quad (7)$$

- Fuel and combustion reactions are modeled using the first-order transfer function with a gas turbine combustion reaction time delay T_{cr} and gas turbine fuel time constant T_f of 0.01 and 0.239 s, respectively.

$$\text{Fuel and combustion reaction} = \frac{-T_{cr} \cdot s + 1}{T_f \cdot s + 1} \quad (8)$$

- Compressor discharge is modeled using the first-order transfer function with compressor discharge volume time constant T_{cd} of 0.2 s.

$$\text{Compressor discharge} = \frac{1}{T_{cd} \cdot s + 1} \quad (9)$$

The governor speed regulation parameters of thermal, hydro, and gas units (R_{hyd} , R_g , and R_{Th}) of 2.4 and the participation factors for each unit (PF_{hyd} , PF_g , and PF_{Th}) are 0.2873, 0.138, and 0.5747, respectively. Table 1 shows the transfer function and parameters for power systems 1 and 2, as well as the T-line.

Table 1. System models and parameters.

Model	Transfer Function	Parameter	Value	Description
Power system 1	$\frac{K_{ps1}}{T_{ps1} \cdot s + 1}$	$T_{ps1} = T_{ps2}$	11.49 s	Power system time constants
Power system 2	$\frac{K_{ps2}}{T_{ps2} \cdot s + 1}$	$K_{ps1} = K_{ps2}$	68.9655	
T-line	$\frac{2\pi T_{12}}{s}$	T_{12}	0.0433	Synchronization factor
		B_1, B_2	0.4312	Coefficient values of frequency bias

2.2. Wind Generation Model

The wind generating unit model was created in a MATLAB-Simulink environment with a white noise block that behaves as a randomized speed that is boosted by wind flow speed, as illustrated in Figure 3. Additionally, the participation factor of the wind system generation unit $\text{PF}_{\text{WT}} = 0.025$. Figure 4 depicts the wind turbine's fluctuating power. The wind generation unit's output power may be calculated using the following equation [44]:

$$P_W = 1/2 \rho A_T V_W^3 C_P(\lambda, \beta) \quad (10)$$

where P_W is the output power of the wind turbine, ρ is the air density in kg/m^3 , A_T is the swept area by the rotor in m^2 , V_W is the wind's nominal speed in m/s , and C_P denotes the rotor's blade parameter. C_P is calculated from the Equation (11) and C_1 to C_7 are the parameters of the turbine.

$$C_P(\lambda, \beta) = C_1 \cdot \left(\frac{C_2}{\lambda_I} - C_3 \beta - C_4 \beta^2 - C_5 \right) \cdot e^{\frac{C_6}{\lambda_I} + C_7 \lambda_T} \quad (11)$$

where β represents the pitch angle of the blade and λ_T indicates the optimal tip speed ratio (TSR), which may be computed using Equation (12).

$$\lambda_T = \lambda_T^{OP} = \frac{\omega_T \cdot r_T}{V_W} \quad (12)$$

where r_T is the radius of the rotor, λ_I is intermittent tip speed ratio as determined by the Equation (13). The nominal wind generation coefficients are displayed in Table 2.

$$\frac{1}{\lambda_I} = \frac{1}{\lambda_T + 0.08 \beta} - \frac{0.035}{\beta^3 + 1} \tag{13}$$

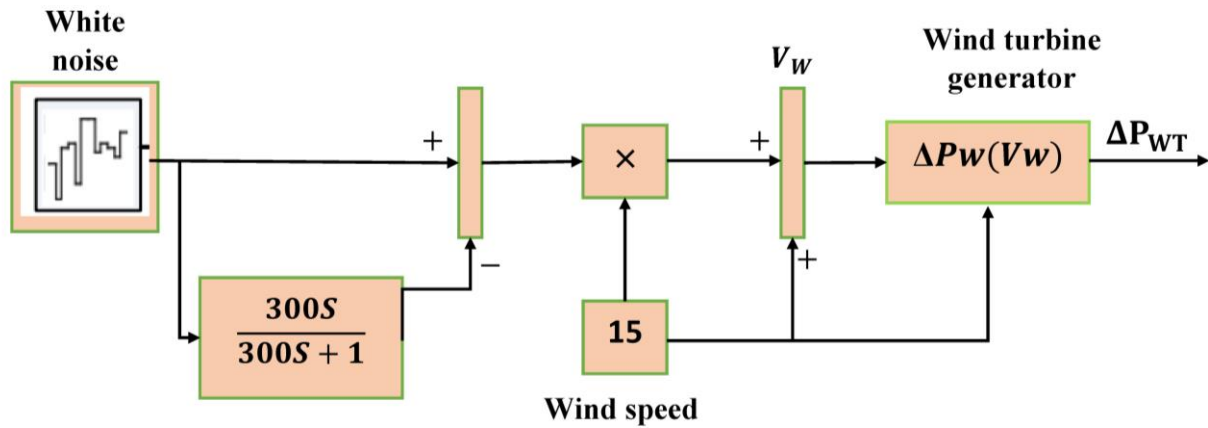


Figure 3. System model for the wind power plant.

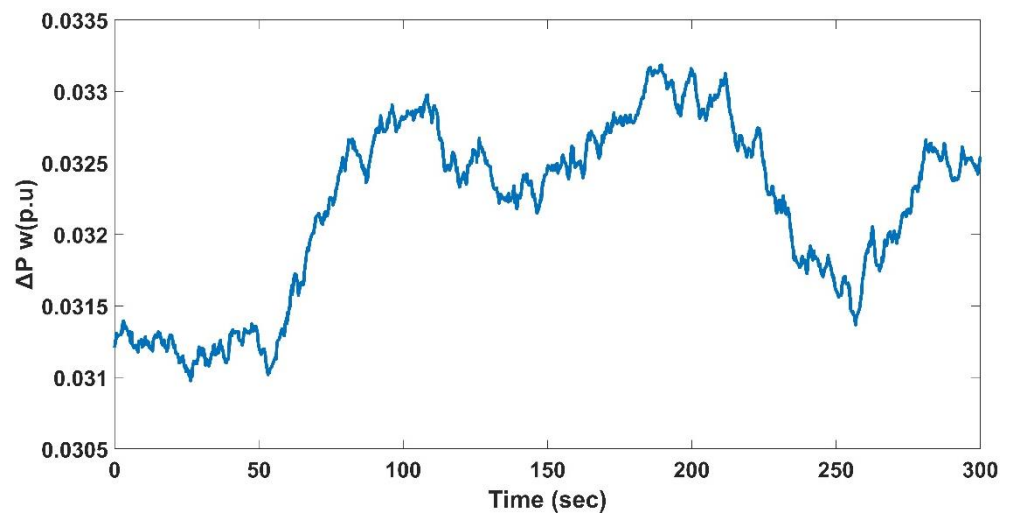


Figure 4. Wind power fluctuations.

Table 2. The wind power plant coefficients.

Parameter	Value	Parameter	Value
P_W	750 kW	C_2	116
V_W	15 m/s	C_3	0.4
r_T	22.9 m	C_4	0
ρ	1.225 kg/m ³	C_5	5
A_T	1684 m ²	C_6	21
λ_T	22.5 r.p.m	C_7	0.1405
C_1	-0.6175		

2.3. PV Generation Model

Weather conditions have a considerable influence on the performance of the PV system’s production, causing it to be erratic. Therefore, significant frequency fluctuations induced by PV output power, threaten the system frequency stability. As a result, power

variations from the solar PV power units may be evaluated by taking the variation from the uniform and non-uniform solar irradiance into account. The power variation of the PV solar system in real life is captured by a white noise block in the MATLAB program, as seen in Figure 5 in the PV solar power system from study [44]. To imitate the real solar power variation, the PV system model's fluctuating output power is calculated using Equation (14) [44]. Figure 6 depicts the PV model's output power. In addition, the participation factor of the PV system generation unit is taken as $PF_{WT} = 0.015$.

$$\Delta P_{Solar} = 0.6\sqrt{P_{Solar}} \quad (14)$$

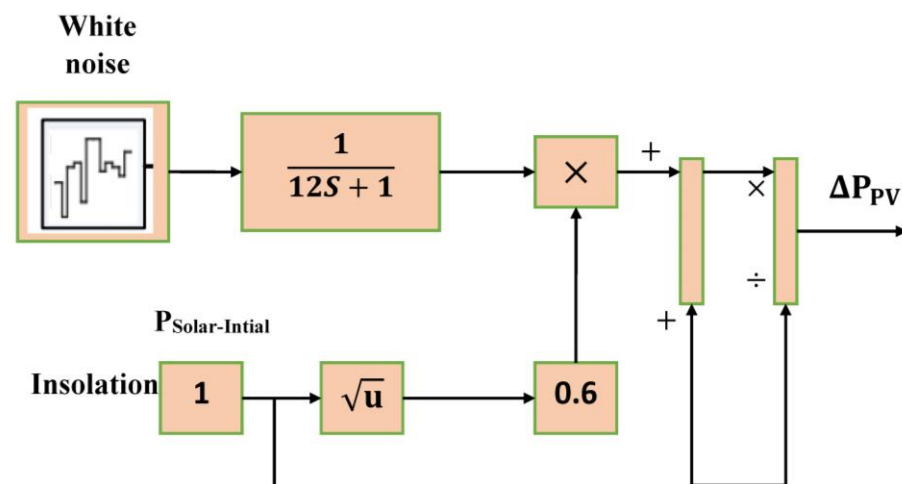


Figure 5. System model for a PV power plant.

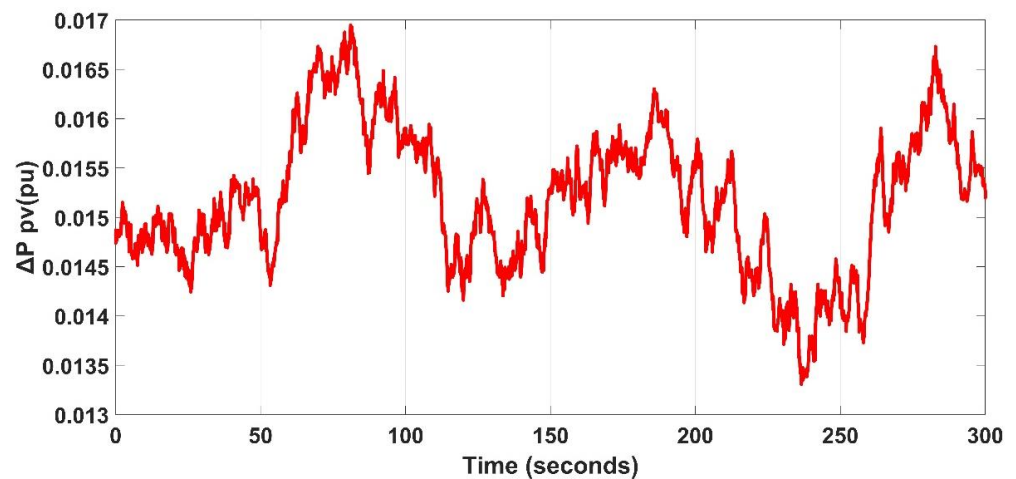


Figure 6. PV power fluctuations.

3. Wild Horse Optimization Algorithm

The wild horse optimization (WHO) is a modern metaheuristic algorithm suggested by Naruei et al. [40] that is based on wild horses' social lives. Wild horses can represent a variety of behaviors in this algorithm, including grazing, mating, hunting, leading, and chasing. Horses are split into two social classes: territory and non-territory. The WHO algorithm, on the other hand, concentrates on non-territorial groupings, which include the group leader, known as the stallion, several mares, and their offspring, the stallion's function is to lead the group and converse with the mares, while the foals begin their life grazing. Furthermore, as foals reach the age of puberty, they leave their groups and join another. The WHO algorithm's procedures can be summarized in the following steps [40].

3.1. Population Initialization

The parameters required for the WHO algorithm are initialized in this stage to evaluate the initial solutions and subsequently changed by the algorithm approach. Horses are organized into groups, and each group has one stallion. Equation (15) can be used to evaluate this division as follows [40]:

$$H = Q \cdot SR \quad (15)$$

where H represents the total number of groups, Q denotes the size of the population, and SR denotes the number of stallions inside the population.

3.2. Grazing Behavior

This step depicts the grazing behavior of foals before they reach puberty. The stallion is seen as being right in the center of the grazing area. In an instance in which the remainder of the members of the group surround the area's center, Equation (16) can be used to represent this behavior [40]:

$$X_{i+1,H}^j = 2Z \cdot \cos(2\pi RZ) \cdot (S^j - X_{i,H}^j) + S^j \quad (16)$$

where i is the group member's number; j denotes the stallions' numbers, $X_{i+1,H}^j$ and $X_{i,H}^j$ represent the position of the group member in the next and current iteration, respectively; Z is a randomly selected adaptive mechanism; R is a random value in the range of $[-2, 2]$; S^j denotes the stallion's position; and Z is calculated from the following equation:

$$\begin{aligned} P = \vec{R}_1 < TDR; \text{IDX} = (P == 0); \\ Z = R_2 \ominus \text{IDX} + R_3 \ominus (\sim \text{IDX}) \end{aligned} \quad (17)$$

where P is a 0 to 1 vector, \vec{R}_1 and \vec{R}_3 are a random value between $[0, 1]$, and IDX indexes of the random vector \vec{R}_1 returns that satisfy the condition $(P == 0)$. R_2 is a uniform random value that has a range of $[0, 1]$. TDR is an adaptive parameter that begins at 1 and declines during the enforcement of the algorithm and reaches 0 at the end of the execution of the algorithm, according to the following Equation [40]:

$$TDR = 1 - it \cdot \frac{1}{\text{maxit}} \quad (18)$$

3.3. Behavior of Horse Mating

This stage demonstrates how foals act as they enter puberty. As previously mentioned, foals leave their groups to join another to mate and to prevent fathers from mating with their daughters and sisters. Furthermore, Equation (19) [40] can be used to express this behavior:

$$X_{H,l}^t = \text{Mean} \left(X_{H,i'}^u, X_{H,j}^w \right) \text{ and } i \neq j \neq l \quad (19)$$

where $X_{H,l}^t$ represents the position of the horse t of group l ; $X_{H,i}^u$ denotes the foal u position in group i ; and $X_{H,j}^w$ the foal w position in group j , in which foal u mates with foal w in the group l . Hence, the necessary condition for mating is achieved.

3.4. Group Leadership

During this phase, the group stallion guides the members of the group to a waterhole for feeding. In addition, the stallion fights with other stallions for dominance of the waterhole. Equation (20) [40] can be used to depict this behavior:

$$S_{i+1,G} = \begin{cases} 2Z \cdot \cos(2\pi RZ) \cdot (WP - S_{i,G}) + WP & \text{if } r_1 > 0.5 \\ 2Z \cdot \cos(2\pi RZ) \cdot (WP - S_{i,G}) - WP & \text{if } r_1 \leq 0.5 \end{cases} \quad (20)$$

where $S_{i+1,G}$, $S_{i,G}$ represent the next and current position of the leader, respectively, WP is the position of the waterhole and r_1 is random vector between $[0, 1]$.

3.5. Leaders Exchange and Selection

Finally, the group leader is selected considering the best fitness value. When the algorithm procedure is completed, a group leader is chosen in each iteration, with the best leader chosen from among the total leaders in the iterations. This phase can be represented by Equation (21) as follows [40]:

$$S_{i,G} = \begin{cases} X_{i,G} & \text{if } \text{cost}(X_{i,G}) < \text{cost}(S_{i,G}) \\ S_{i,G} & \text{if } \text{cost}(X_{i,G}) > \text{cost}(S_{i,G}) \end{cases} \quad (21)$$

Table 3 also provides the WHO algorithm parameter setting values for this study. The WHO algorithm flowchart is shown in Figure 7.

Table 3. Setting values for the WHO parameters [45].

WHO Parameter	Value
SR	0.2
H	6
Q	30
Number of foals	24
R	0.2372
WP	[2, 1.83, 0, 2, 2, 2, 0, 0, 0, 1, 0, 0, 0, 4.7, 20, 20, 3.19, 20, 20, 12.7]

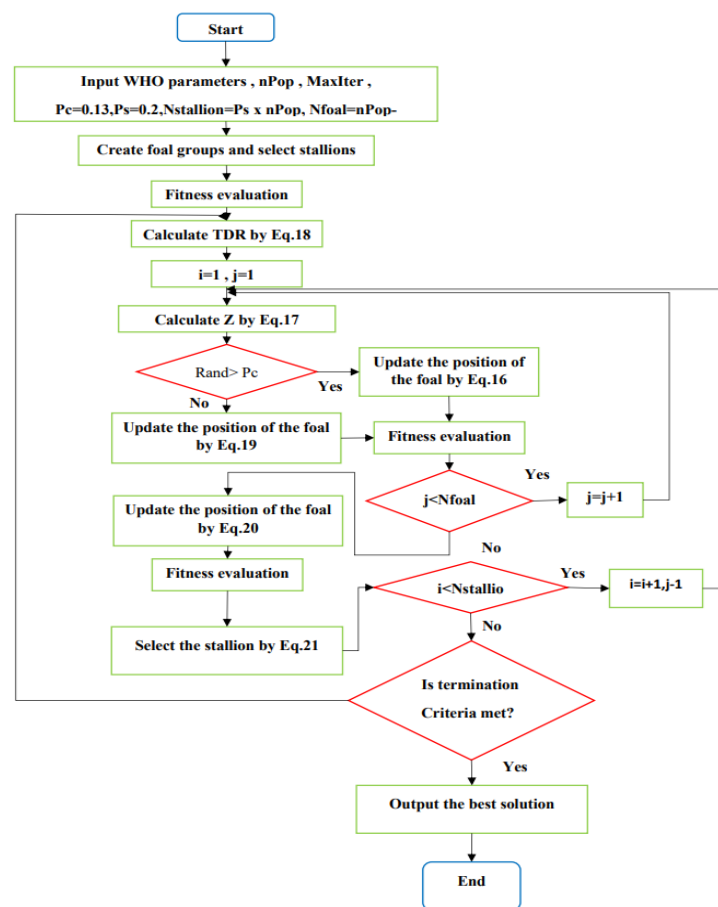


Figure 7. Flowchart of the WHO algorithm [40].

4. Structure of the Controller and Problem Formulation

The primary purpose of the new structure of the PIDD²-PD suggested controller is to manage and improve the frequency response of a power system consisting of a multi-source when it is confronted with sudden load variations and renewable energy source fluctuations. The controller is proposed in both areas to decrease frequency deviations (ΔF_1 , ΔF_2) and the tie-line power deviation between both areas ($\Delta P_{\text{tie-line}}$) for different load perturbations and renewable energy sources.

Figure 8 depicts the combined controller structure's schematic diagram. It has the potential to lessen the impact of disturbances $d(s)$ on the performance of the control system. Furthermore, the primary loop transfer function could be expressed by Equation (22).

$$Y(s) = G(s)U(s) + d(s) \quad (22)$$

where $G(s)$ indicates the operation and $U(s)$ is the input signal to $G(s)$. $U(s)$ can be calculated by Equation (23)

$$U(s) = C_1(s) \cdot C_2(s) \quad (23)$$

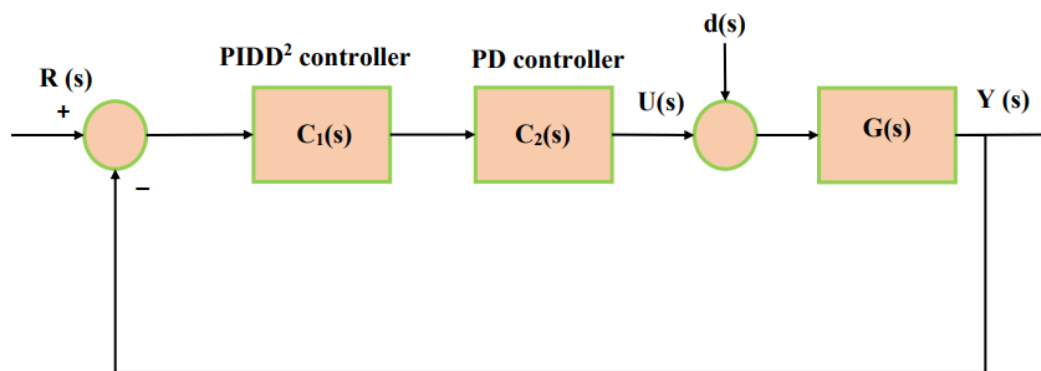


Figure 8. Combined controller block diagram.

In this hybrid power system case study, the controller utilized for both areas is a PIDD²-PD controller. Researchers have commonly employed the traditional PID controller because of its ease of design and operating efficiency. The PIDD² structure is identical to that of standard PID but also with the addition of second-order derivative gain [46]. The transfer functions of the PIDD² and PD controller can be represented using Equation (24), and Equation (25), respectively, as follows:

$$C_1(s) = KP + \frac{KI}{s} + KD \left[\frac{N_d \cdot s}{s + N_d} \right] + KD \left[\frac{N_d \cdot s}{s + N_d} \right] \cdot KDD \left[\frac{N_{dd} \cdot s}{s + N_{dd}} \right] \quad (24)$$

$$C_2(s) = kp + kd \left[\frac{nf \cdot s}{s + nf} \right] \quad (25)$$

where $(KP, KI, (KD, KDD)$ and (N_d, N_{dd})) are the (proportional gain, integral gain, derivative gains, filters' coefficients) of the PIDD² controller, in addition, $((kp)$ is the proportional gain, (kd) is the derivative gain, and (nf) is the filter coefficient) of the PD controller. The structure of a PIDD²-PD is depicted in Figure 9.

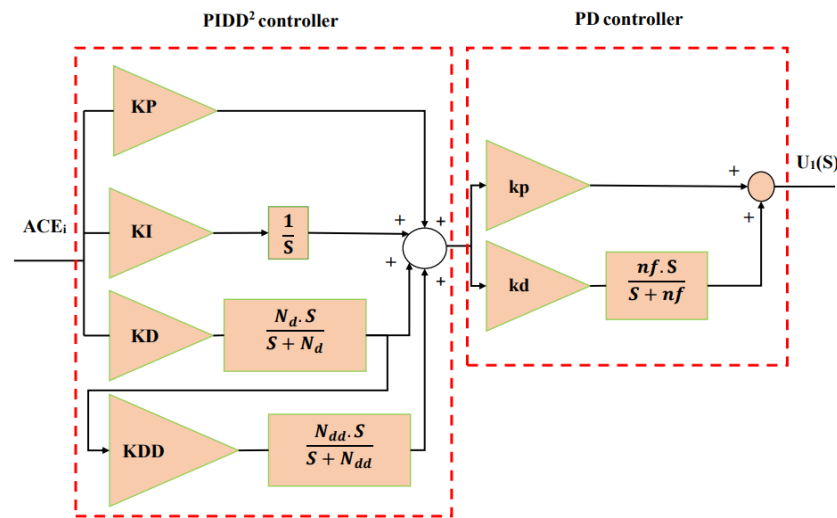


Figure 9. The suggested PIDD²-PD structure.

Using the WHO algorithm, the optimum PIDD²-PD controller parameters will be determined by reducing the fitness function (FF). The integral of time multiplied by the squared error (ITSE) is selected as the fitness function since it can minimize the settling time and quickly suppress the high oscillation [31]:

$$ITSE = \int_0^{T_{sim}} t [\Delta F_1^2 + \Delta F_2^2 + \Delta P_{12}^2] dt \tag{26}$$

where T_{sim} stands for simulation time, the controller parameters are constrained as follows:

$$\left\{ \begin{array}{l} KP_{min} \leq KP \leq KP_{max} \\ KI_{min} \leq KI \leq KI_{max} \\ KD_{min} \leq KD \leq KD_{max} \\ KDD_{min} \leq KDD \leq KDD_{max} \\ kp_{min} \leq kp \leq kp_{max} \\ kd_{min} \leq kd \leq kd_{max} \\ N_d \min \leq N_d \leq N_d \max \\ N_{dd} \min \leq N_{dd} \leq N_{dd} \max \\ nf_{min} \leq nf \leq nf_{max} \end{array} \right. \tag{27}$$

For all scenarios, the lower limits are set [0, 0, 0, 0, 0, 0, 100, 100, 100] while the higher limits are set [50, 50, 50, 0.8, 50, 50, 500, 500, 500].

5. Results of Simulation and Discussions

In this part, the performance of the hybrid power system is studied, consisting of two areas tested in multiple scenarios, such as various load perturbations (step, random, multi-step), renewable energy source penetration, and system parameter variations. The evaluation of the suggested PIDD²-PD controller optimized by the WHO algorithm is compared against the ID-T and PID-TID controllers optimized by the WHO and the ID-T controller optimized by the AOA under different operating conditions.

5.1. Performance Analysis of the WHO

This section verifies the wild horse algorithm competency based on the load frequency control (LFC) study. The verification of the proposed WHO optimization’s efficiency and performance is assessed by contrasting it to the performance of different optimization strategies from the literature, like ChOA [41] and WOA [42]. The comparison is performed based on optimizing the designed controller settings to improving the frequency stability of

the studied network power system, consisting of two areas fed by various energy sources, considering the SLD is supplied to the first area with a 1% value. The maximum number of iterations and the number of the population is specified to be 50 and 30, respectively.

As a result, Table 4 summarizes the optimal settings for the PIDD²-PD-constructed controller as determined by the three optimization strategies employed in this study: WOA, ChOA, and WHO.

Table 4. Optimum settings of the suggested PIDD²-PD controller are optimized by three optimization algorithms (WOA, ChOA, WHO).

AREA 1									
Algorithm	PD ₁			PIDD ₁ ²					
	kp ₁	kd ₁	nf ₁	KP ₁	KI ₁	KD ₁	KDD ₁	Nd ₁	Ndd ₁
WOA	14.253	4.4785	500	50	50	1.7171	0.1	500	500
ChOA	14.564	0	500	50	0	6.3209	0.1228	401.6571	309.896
WHO	38.475	0.0144	431.882	41.1532	0.3835	5.6677	0.1	100	478.5245
AREA 2									
Algorithm	PD ₂			PIDD ₂ ²					
	kp ₂	kd ₂	nf ₂	KP ₂	KI ₂	KD ₂	KDD ₂	Nd ₂	Ndd ₂
WOA	50	50	500	50	12.451	4.1011	0.8	500	500
ChOA	0.008	0	496.631	0.0975	0.1436	0	0.2725	323.829	304.0149
WHO	0	17.32	334.76	50	7.8044	0.5505	0.1501	251.83	498.7457

Figure 10 depicts the convergence curve for the three algorithms. By comparing the effectiveness of the WHO technique with that of ChOA and WOA, the WHO algorithm can be demonstrated to have superior convergence to other algorithms. The dynamic response of the system is shown in Figure 11. It can be deduced that the suggested controller optimized by the WHO algorithm has the best performance in reducing undershoot, overshoot, and settling time and the objective function ITSE as well as improving the dynamic response compared to the attained from the suggested controller based on WOA and ChOA algorithms, as shown in Table 5.

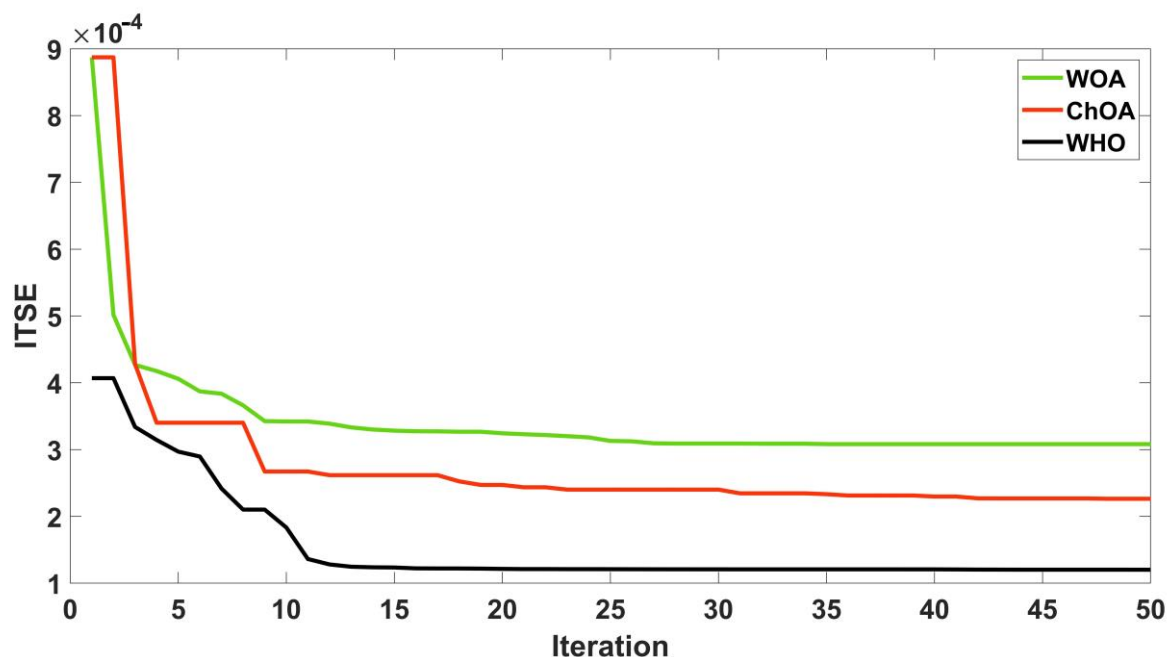


Figure 10. The convergence curve for (WHO, ChOA, WOA) optimization techniques.

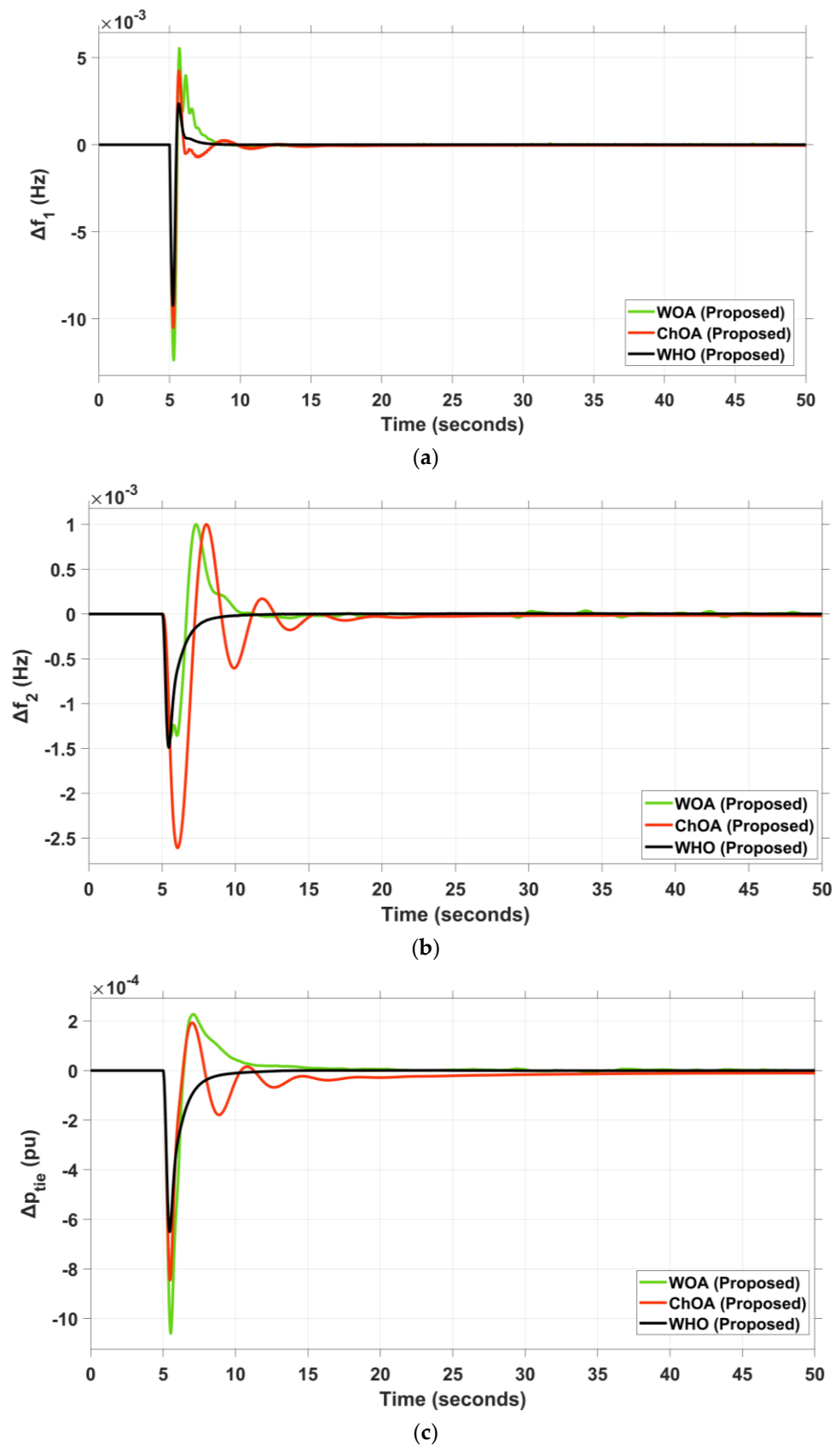


Figure 11. Dynamic power system response: (a) Δf_1 , (b) Δf_2 , and (c) Δp_{tie} .

Table 5. Dynamic system response using (WOA, ChOA, and WHO) optimization techniques.

Optimization Techniques	ΔF_1 (Hz)			ΔF_2 (Hz)			ΔP_{tie} (p.u)			ITSE
	Max. OS	Max. US	Set-Time	Max. OS	Max. US	Set-Time	Max. OS	Max. US	Set-Time	
WOA	0.0055	0.0124	3.6	0.001	0.00137	15.1	0.00023	0.00106	12.8	0.0003082
ChOA	0.0042	0.0105	10.7	0.001	0.00261	20.8	0.00019	0.00085	28	0.0002264
WHO (proposed)	0.0024	0.0092	3.3	0	0.00149	7.2	0	0.00065	8.8	0.0001202

Figure 11 shows the system responses to (a) frequency deviation in Area-1 (ΔF_1), (b) frequency deviation in Area-2 (ΔF_2), and (c) tie-line power deviation (ΔP_{tie}) for load disturbances in both areas using different optimization algorithms. The PIDD²-PD controller based on the WHO response has the lowest undershoot and overshoot than the other techniques, which are (9.2×10^{-3}) Hz and (2.4×10^{-3}) Hz for ΔF_1 , respectively (see Figure 11a), and 1.49×10^{-3} Hz undershoot for ΔF_2 with no overshoot (see Figure 11b). Additionally, the WHO application has a lowest undershoot and overshoot than the other cases when considering the tie-line power deviation (ΔP_{tie}), which equals 6.5×10^{-4} p.u for ΔP_{tie} (see Figure 11c). Moreover, the WHO response has the lowest settling time than the other two techniques, which is 3.3 s for ΔF_1 and 7.2 s for ΔF_2 . Additionally, the WHO application has the lowest settling time than the other cases when considering the tie-line power deviation (ΔP_{tie}), which equals 8.8 s for ΔP_{tie} .

5.2. Simulation Results and Discussions

The simulation results for the studied power system with various power sources are performed using the computer programming MATLAB-Simulation to verify the suggested controller's effectiveness in improving the studied system's performance. The simulation is arranged in the following manner:

- Scenario I: Evaluation of system dynamic response under load variation types;
- Scenario II: Evaluation of system dynamic response using RESs disturbances;
- Scenario III: Evaluation of system dynamic response with RESs disturbances, taking into consideration the communication time delay (CTD), applied to the proposed controller output;
- Scenario IV: Evaluation of system dynamic response based on RESs disturbances and changes in system settings.

5.2.1. Scenario I: Evaluation of System Dynamic Response under Load Variation Types

This scenario included applied load variation types (i.e., SLD, MSLD, and RLD) to the investigated power system (see Figure 1) all penetrations are applied in the first area. Additionally, this scenario is subdivided into three sections.

Section A: Performance evaluation of the system under 1% SLD step load disturbances.

In this section, the testing of the power system studied is performed under 1% SLD applied in the first area occurred after 5 s. SLD may be represented in the power system by detaching certain generators, resulting in outages caused by the shutdown of all generators at the stations. Furthermore, in this case, the performance efficiency of the proposed PIDD²-PD controller optimized by the WHO algorithm is compared to the performance efficiency of other controllers, such as WHO-optimized ID-T [31], PID-TID [32] controllers and ID-T controller optimized by the AOA algorithm [31]. Table 6 displays the settings of the controllers considered in this section.

Table 6. The optimum settings of the controllers in Scenario I, Section A.

AREA 1									
Algorithm	PD ₁			PIDD ₁ ²					
	kp ₁	kd ₁	nf ₁	KP ₁	KI ₁	KD ₁	KDD ₁	Nd ₁	Ndd ₁
PIDD ² -PD (WHO) (suggested)	38.475	0.0144	431.882	41.1532	0.3835	5.6677	0.1	100	478.5245
AREA 2									
Algorithm	PD ₂			PIDD ₂ ²					
	kp ₂	kd ₂	nf ₂	KP ₂	KI ₂	KD ₂	KDD ₂	Nd ₂	Ndd ₂
PIDD ² -PD (WHO) (suggested)	0	17.32	334.76	50	7.8044	0.5505	0.1501	251.83	498.7457
AREA 1									
Algorithm	PID				TID				
	kp ₁	ki ₁	kd ₁	nf ₁	KT ₁	n ₁	KI ₁	KD ₁	
PID-TID (WHO)	6.1095	0	34.0678	489.8079	49.9998	2.5167	50	2.5459	
AREA 2									
Algorithm	PID				TID				
	kp ₂	ki ₂	kd ₂	nf ₂	KT ₂	n ₂	KI ₂	KD ₂	
PID-TID (WHO)	25.6245	12.8848	3.2186	499.8395	49.2407	2.4475	14.9894	3.8772	
AREA 1									
Algorithm	T				ID				
	KT ₁		n ₁		KI ₁		KD ₁		NC ₁
ID-T (WHO)	−31.4909		1.7755		39.3266		25.3455		499.3504
AREA 2									
Algorithm	T				ID				
	KT ₂		n ₂		KI ₂		KD ₂		NC ₂
ID-T (WHO)	−15.2490		2.8479		38.8390		12.0328		336.9504
AREA 1									
Algorithm	T				ID				
	KT ₁		n ₁		KI ₁		KD ₁		NC ₁
ID-T (AOA)	−4.9		2.17		−3.4		−3.6		496.9
AREA 2									
Algorithm	T				ID				
	KT ₂		n ₂		KI ₂		KD ₂		NC ₂
ID-T (AOA)	−0.002		6.07		−0.010		−2.390		469.2

From Table 7 and Figure 12, it can be seen that applied step load disturbances in the first area initially result in a decrease in the system's dynamic performance. Employing the ID-T controller optimized by the WHO technique is better than using the ID-T controller and is improved by the AOA technique for damping system oscillations. The proposed PIDD²-PD controller optimized by the WHO algorithm has the lowest overshoot, undershoot, and settling time of the other three controllers and provides the best objective function based on ITSE, which is 1.202×10^{-4} .

Table 7. Dynamic system response under effect Scenario I, Section A.

Controller	ΔF_1 (Hz)			ΔF_2 (Hz)			ΔP_{tie} (p.u)			ITSE
	Max. OS	Max. US	Set-Time	Max. OS	Max. US	Set-Time	Max. OS	Max. US	Set-Time	
PIDD ² -PD (WHO) (suggested)	0.0024	0.0092	3.3	0	0.00149	7.2	0	0.00065	8.7	0.0001202
PID-TID (WHO)	0.0013	0.0112	16.1	0.00021	0.00235	18.6	0.00009	0.00096	20.4	0.0002403
ID-T (AOA)	0.009	0.028	11	0.005	0.024	12	0.001	0.004	11	0.001
ID-T (WHO)	0.0042	0.0103	11.8	0.00098	0.00272	13.3	0.00017	0.00091	16	0.0002689

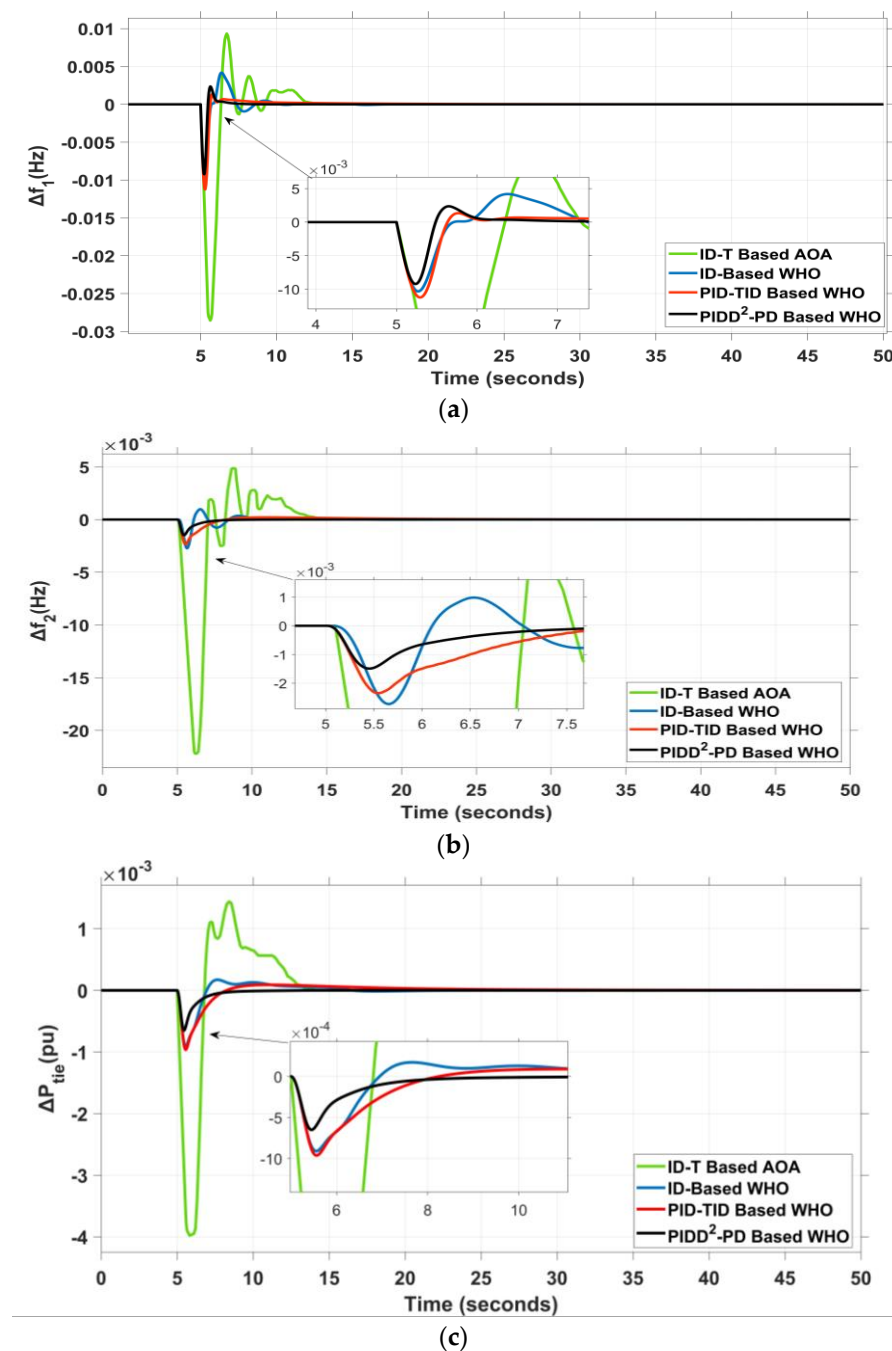


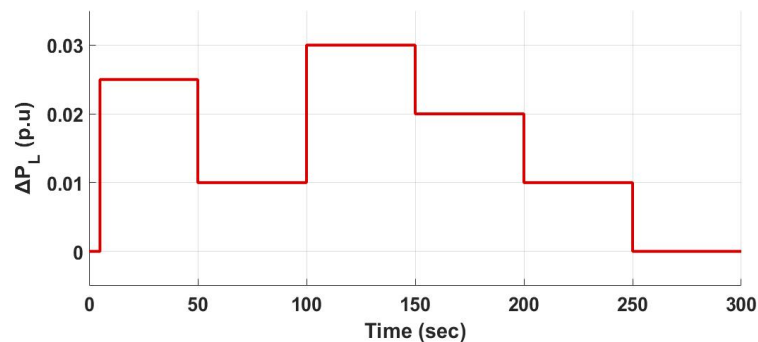
Figure 12. Dynamic power system response under scenario I, Section A: (a) ΔF_1 , (b) ΔF_2 , and (c) ΔP_{tie} .

Section B: Performance evaluation of the system under multi-step load disturbances MSLD.

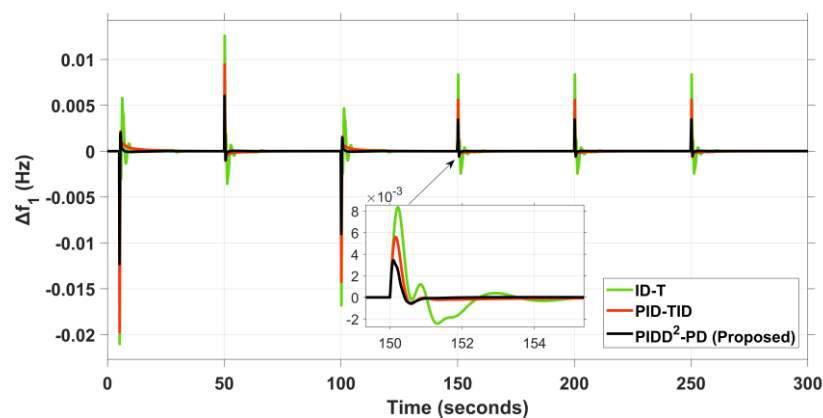
In this section, an MSLD is used to mimic a realistic load variation in the analyzed two-area power system, where the MSLD is shown in Figure 13a. MSLD is denoted as a series-forced shutdown of generators or an unexpected switch of loading. The effectiveness of the suggested PIDD²-PD controller based on the WHO algorithm has been tested and assessed by applying a series of load changes in the first area and comparison with using several control strategies (i.e., PID-TID and ID-T controllers based on the WHO). Figure 13 depicts the dynamic system response. Table 8 also shows the dynamic response of the power system in this part. As a result, the proposed PIDD²-PD controller has the lowest undershoot, overshoot, settling time, and ITSE. The superiority of the proposed suggested PIDD²-PD controller based on WHO over the other controllers optimized using the WHO algorithm is that with the proposed PIDD²-PD controller it is possible to get a greater decrease in system frequency variations and power flow in the tie line compared to other controllers in this case. Therefore, the developed PIDD²-PD enhances the system's reliability.

Table 8. Dynamic system response under effect Scenario I, Section B.

Controller	ΔF_1 (Hz)		ΔF_2 (Hz)		ΔP_{tie} (p.u)		ITSE
	Max. OS	Max. US	Max. OS	Max. US	Max. OS	Max. US	
PIDD ² -PD (WHO) (suggested)	0.0060	0.0123	0.00076	0.00154	0.00033	0.00067	0.003442
PID-TID (WHO)	0.0095	0.0197	0.00146	0.00324	0.00059	0.00130	0.01051
ID-T (WHO)	0.0126	0.0210	0.0029	0.0049	0.00096	0.00161	0.02664



(a)



(b)

Figure 13. Cont.

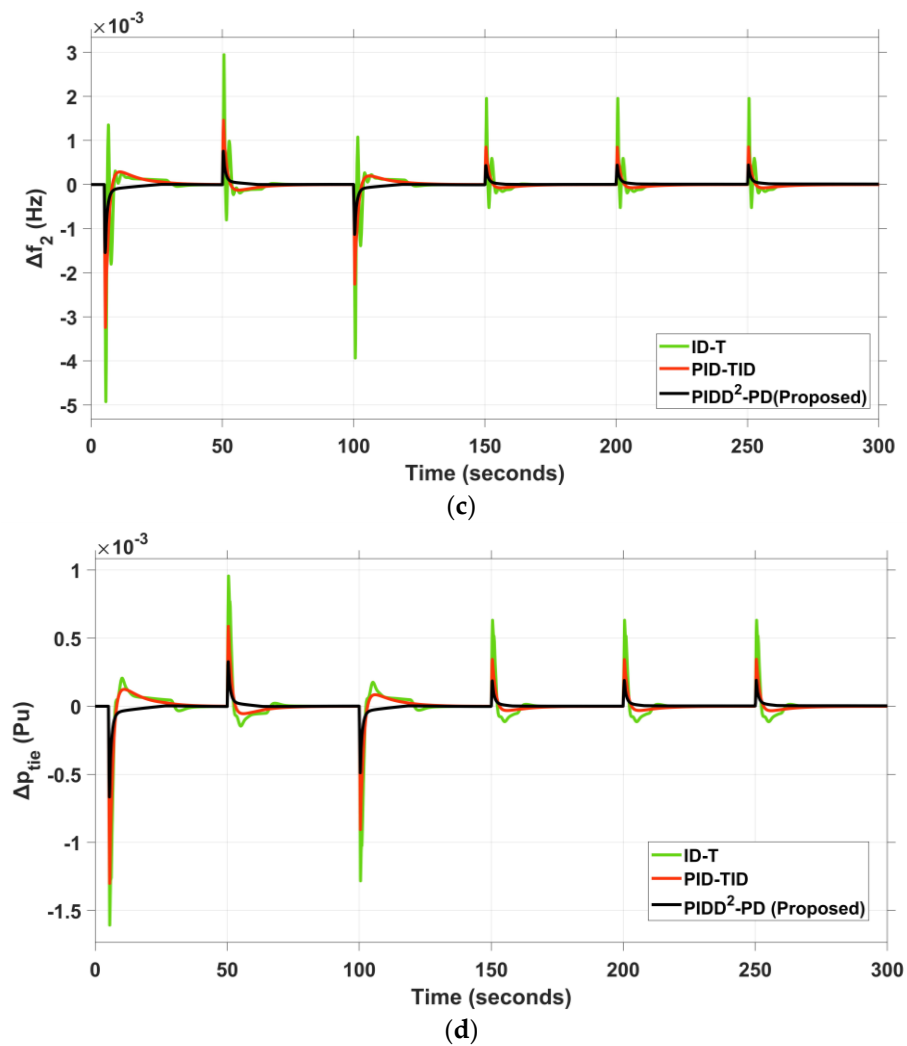


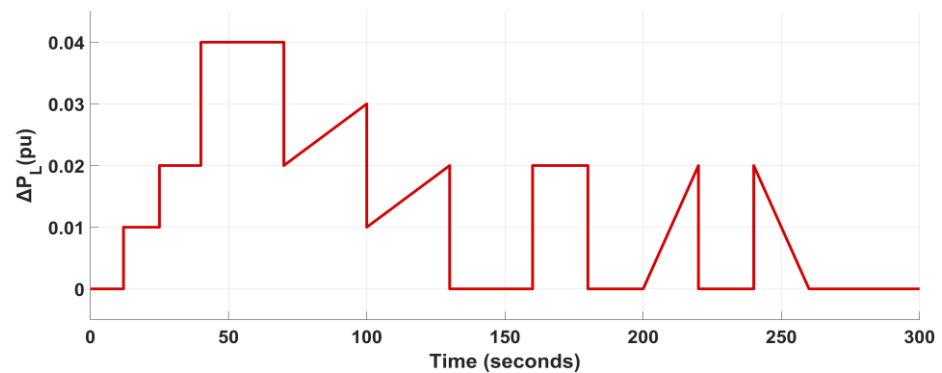
Figure 13. Dynamic power system response under Scenario I, Section B: (a) MSLD, (b) ΔF_1 , (c) ΔF_2 , and (d) ΔP_{tie} .

Section C: Performance evaluation of the system under random load disturbances RLD.

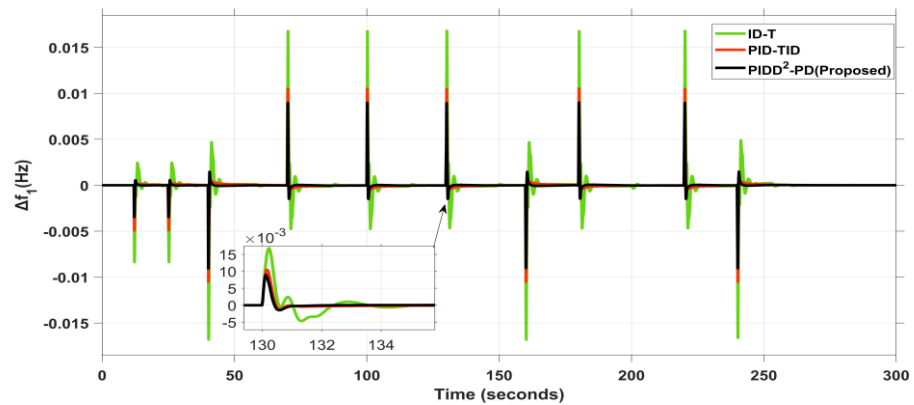
After evaluating the efficiency of the suggested PIDD²-PD controller in the two prior situations, RLD is a varied collection of series disturbances that may be represented by industrial loads linked to a power system network. Random load disturbances are applied to the first area shown in Figure 14a. Additionally, Figure 14 depicts the system reaction for this section using several control strategies (i.e., PIDD²-PD, PID-TID, and ID-T controllers based on the WHO). Table 9 summarizes the dynamic performance of the system in this part. In comparison to the ID-T and PID-TID controllers, the suggested PIDD²-PD controller based on the WHO has high performance in dealing with rapid and gradual load fluctuations, and the suggested controller shows better performance. It is evident that it dampens the oscillations very fast, with the lowest undershoot and overshoot, in addition to better control quality. This shows that the PIDD²-PD based on the WHO technique is a robust controller used to load frequency control LFC.

Table 9. Dynamic system response under effect Scenario I, Section C.

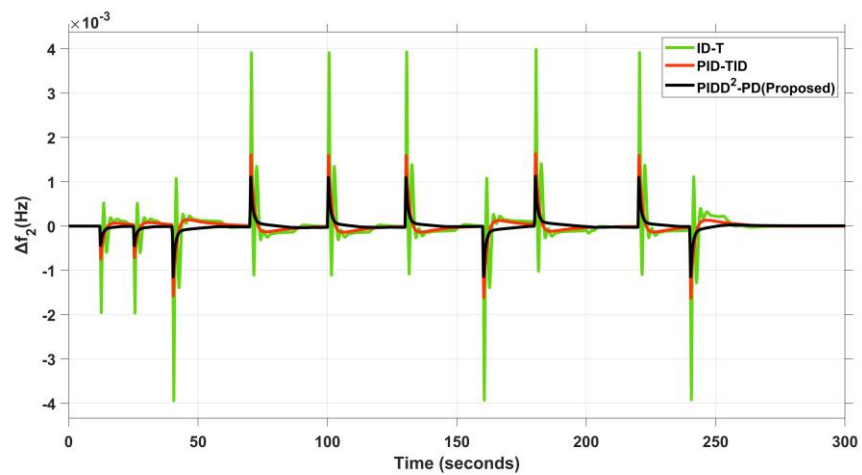
Controller	ΔF_1 (Hz)		ΔF_2 (Hz)		ΔP_{tie} (p.u)		ITSE
	Max. OS	Max. US	Max. OS	Max. US	Max. OS	Max. US	
PIDD ² -PD (WHO) (suggested)	0.0090	0.0091	0.00113	0.00115	0.00049	0.00050	0.01756
PID-TID (WHO)	0.0105	0.0105	0.00164	0.00163	0.00066	0.00065	0.02848
ID-T (WHO)	0.0168	0.0168	0.0040	0.0039	0.00131	0.00129	0.1063



(a)



(b)



(c)

Figure 14. Cont.

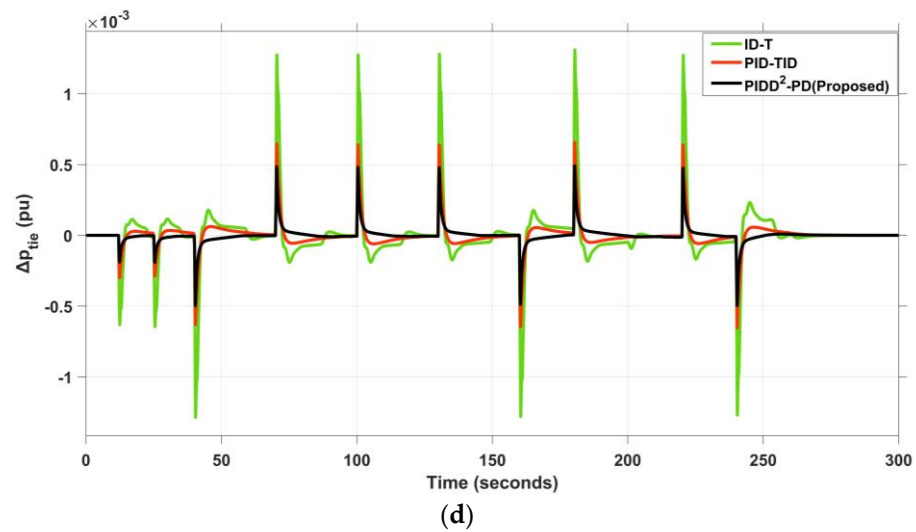


Figure 14. Dynamic power system response under scenario I, Section C: (a) RLD, (b) ΔF_1 , (c) ΔF_2 , and (d) ΔP_{tie} .

5.2.2. Scenario II: Performance Evaluation Based on RESs Penetration

This scenario clarifies the dynamic response of the power system studied shown in Figure 2, considering RESs disturbances depicted in Figures 4 and 6, respectively, using several control strategies (i.e., PIDD²-PD, PID-TID, and ID-T controllers based on the WHO). Figure 15 shows the convergence characteristics of the three controllers. The evaluation by applying a series load of disturbances is shown in Figure 16a to the first area, the PV solar unit with 50 MW is linked to the first area at 250 s, and the wind farm unit with 70 MW rated power is linked to the second area at 100 s, with the note wind farm and the PV solar unit are illustrated in Figures 3 and 5, respectively. Furthermore, Table 10 shows the PIDD²-PD, PID-TID, and ID-T parameters. The maximum number of iterations and the number of the population are specified to be 50 and 30, respectively. Figure 16 illustrates the dynamic power system response and the frequency deviation of the power system network (ΔF_1 , ΔF_2), the tie-line power deviation because of the series load disturbances and the RESs penetration in this scenario. The severe fluctuations in frequency and flow power in the tie-line power occur throughout the period the RESs are connected, as shown in Figure 16. Table 11 summarizes the dynamic performance of the power system. The proposed PIDD²-PD controller can effectively dampen fluctuations in frequency and the flow power in the tie-line power. Furthermore, it obtains the lowest values for both overshoot, undershoot, settling time, and ITSE compared to the PID-TID and ID-T controllers and it has the best convergence characteristics. Additionally, this can be concluded that the ID-T controller is the least effective at controlling RESs variations with the series load disturbances.

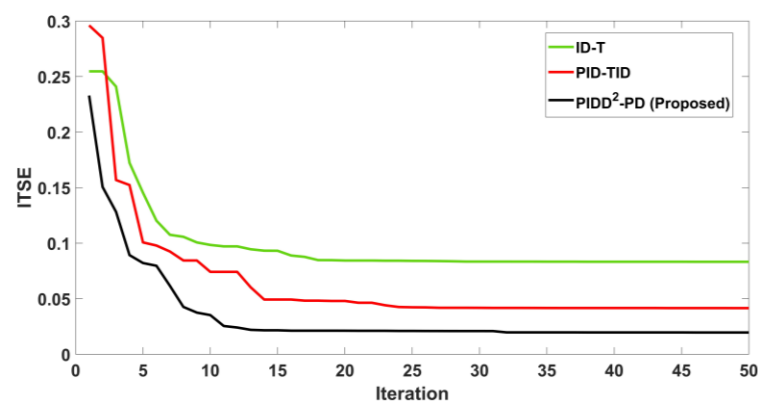


Figure 15. The convergence curve of the three controllers in scenario (II).

Table 10. The Optimum settings of the controllers in Scenario II.

AREA 1									
Algorithm	PD ₁			PIDD ² ₁					
	kp ₁	kd ₁	nf ₁	KP ₁	KI ₁	KD ₁	KDD ₁	Nd ₁	Ndd ₁
PIDD ² -PD (WHO) (suggested)	48.2812	6.328	343.1941	40.63	2.5682	2.1527	0.0084	140.5213	421.9369
AREA 2									
Algorithm	PD ₂			PIDD ² ₂					
	kp ₂	kd ₂	nf ₂	KP ₂	KI ₂	KD ₂	KDD ₂	Nd ₂	Ndd ₂
PIDD ² -PD (WHO) (suggested)	49.9496	2.0937	301.5396	44.5887	9.9736	9.8294	0	420.2037	118.7231
AREA 1									
Algorithm	PID				TID				
	kp ₁	ki ₁	kd ₁	nf ₁	KT ₁	n ₁	KI ₁	KD ₁	
PID-TID (WHO)	23.4461	0	26.4650	300	45.3144	2.5099	14.3536	0.9136	
AREA 2									
Algorithm	PID				TID				
	kp ₂	ki ₂	kd ₂	nf ₂	KT ₂	n ₂	KI ₂	KD ₂	
PID-TID (WHO)	33.2919	0.0947	3.9765	483.1653	40.6655	6.9517	0	2.4108	
AREA 1									
Algorithm	T			ID					
	KT ₁		n ₁	KI ₁		KD ₁		NC ₁	
ID-T (WHO)	−39.9993		1.8675	39.9995		40		500	
AREA 2									
Algorithm	T			ID					
	KT ₂		n ₂	KI ₂		KD ₂		NC ₂	
ID-T (WHO)	−25.3571		9.9994	39.9404		28.3108		495.5133	

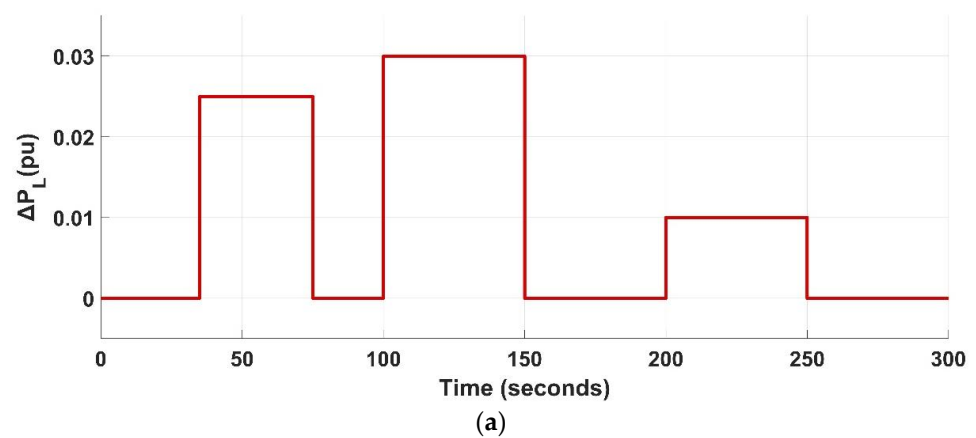


Figure 16. Cont.

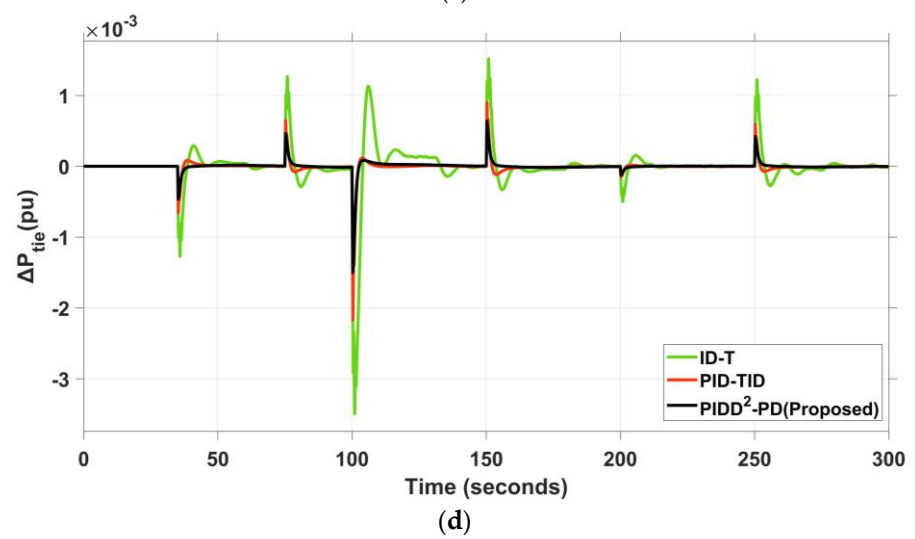
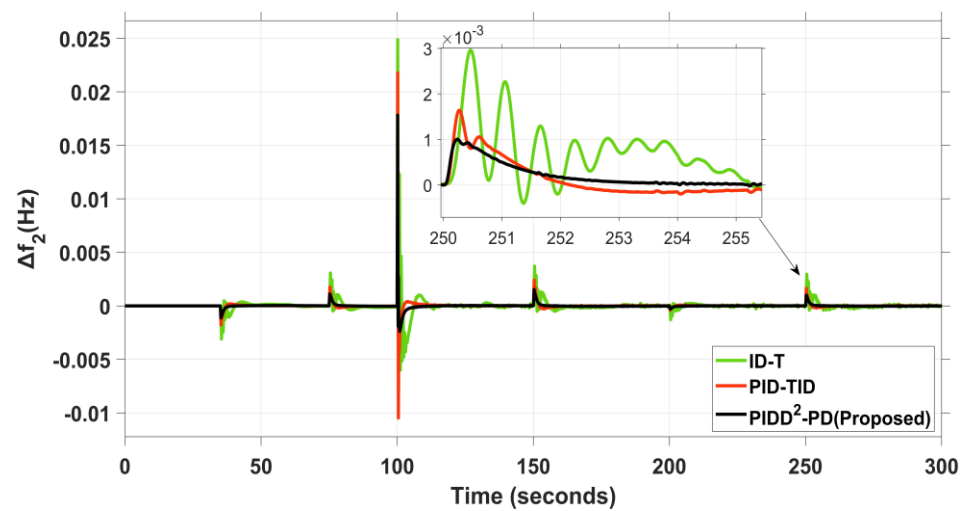
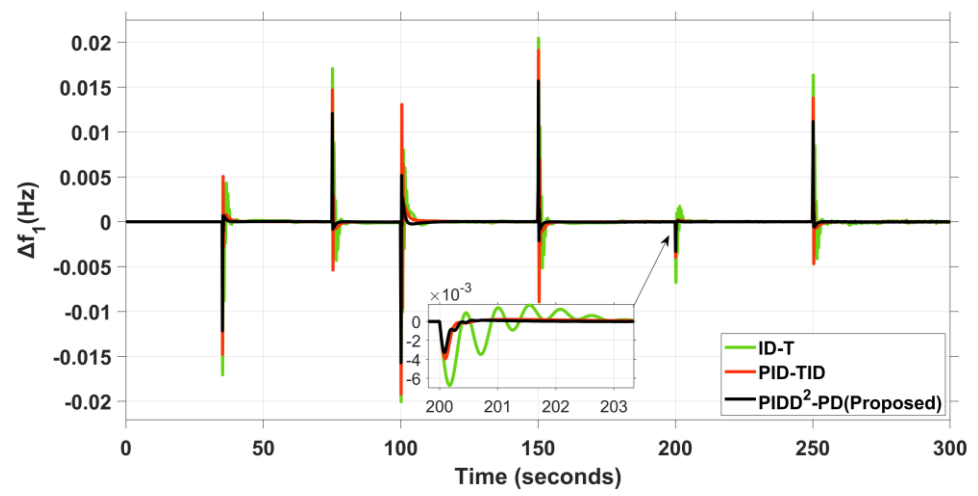


Figure 16. Dynamic power system response under Scenario II: (a) Series load disturbances, (b) ΔF_1 , (c) ΔF_2 , and (d) ΔP_{tie} .

Table 11. Dynamic system response under effect Scenario II.

Controller	ΔF_1 (Hz)		ΔF_2 (Hz)		ΔP_{tie} (p.u)		ITSE
	Max. OS	Max. US	Max. OS	Max. US	Max. OS	Max. US	
PIDD ² -PD (WHO) (suggested)	0.0157	0.0157	0.0178	0.0024	0.00064	0.0015	0.01959
PID-TID (WHO)	0.0191	0.0192	0.0218	0.0105	0.00090	0.00217	0.04153
ID-T (WHO)	0.0205	0.0200	0.0249	0.0077	0.00152	0.00349	0.08325

5.2.3. Scenario III: Evaluation of Performance Using RESs Disturbances and Communication Time Delay (CTD) on the Signal Output of the Controller

This scenario comprises an endurance test in which RESs are penetrated in two areas of the analyzed power system. The PV solar system is linked at 80 s, while the wind farm is linked at 220, and applying step load fluctuation to areas 1 and 2 with values of 0.01 p.u at 10 s and 0.05 p.u at 150 s, respectively. Using CTD on the output controllers with the duration set to 0.1 s, Table 12 summarizes the parameters of the three controllers (PIDD²-PD, PID-TID, and ID-T) optimized by the WHO algorithm, and Table 13 depicts the dynamic performance of the system in this scenario. Figure 17 clarifies the convergence curve of the controllers. Figure 18 depicts the frequency fluctuation of both areas of the power system network studied and flow power in the tie-line power. Due to RESs sources disturbances and applying a communication time delay, the system's response has severely oscillated. The suggested PIDD²-PD controller, on the other hand, can achieve adequate stability of the system power network and significantly reduce the impact of system fluctuation, and obtained the lowest overshoot, undershoot, settling time, and ITSE values than the PID-TID and ID-T controllers shown in Table 13 and Figure 18.

Table 12. The optimum settings of the controllers in Scenario III.

AREA 1									
Algorithm	PD ₁			PIDD ² ₁					
	kp ₁	kd ₁	nf ₁	KP ₁	KI ₁	KD ₁	KDD ₁	Nd ₁	Ndd ₁
PIDD ² -PD (WHO) (suggested)	2.7227	0.3027	195.6591	19.6364	6.3706	7.6158	0.0541	190.8568	130.8450
AREA 2									
Algorithm	PD ₂			PIDD ² ₂					
	kp ₂	kd ₂	nf ₂	KP ₂	KI ₂	KD ₂	KDD ₂	Nd ₂	Ndd ₂
PIDD ² -PD (WHO) (suggested)	7.4519	1.5539	148.7560	6.4190	12.1799	1.8329	0.0269	141.0946	100.4050
AREA 1									
Algorithm	PID				TID				
	kp ₁	ki ₁	kd ₁	nf ₁	KT ₁	n ₁	KI ₁	KD ₁	
PID-TID (WHO)	1.9950	0.0027	4.3505	375.0716	16.9318	1.738	3.4679	1.4928	
AREA 2									
Algorithm	PID				TID				
	kp ₂	ki ₂	kd ₂	nf ₂	KT ₂	n ₂	KI ₂	KD ₂	
PID-TID (WHO)	7.3223	0.0140	3.2081	312.8155	7.5334	5.1325	3.9343	1.1741	

Table 12. Cont.

AREA 1					
Algorithm	T		ID		
	KT ₁	n ₁	KI ₁	KD ₁	NC ₁
ID-T (WHO)	-5.4107	9.5456	5.0845	6.6880	389.4373
AREA 2					
Algorithm	T		ID		
	KT ₂	n ₂	KI ₂	KD ₂	NC ₂
ID-T (WHO)	-17.4930	1.4958	4.5823	13.7478	480.3091

Table 13. Dynamic system response under effect Scenario III.

Controller	ΔF_1 (Hz)		ΔF_2 (Hz)		ΔP_{tie} (p.u)		ITSE
	Max. OS	Max. US	Max. OS	Max. US	Max. OS	Max. US	
PIDD ² -PD (WHO) (suggested)	0.0148	0.0116	0.030	0.048	0.00308	0.00176	0.1488
PID-TID (WHO)	0.0222	0.0246	0.044	0.078	0.0075	0.0035	0.5603
ID-T (WHO)	0.0323	0.0307	0.052	0.080	0.0088	0.0055	0.9892

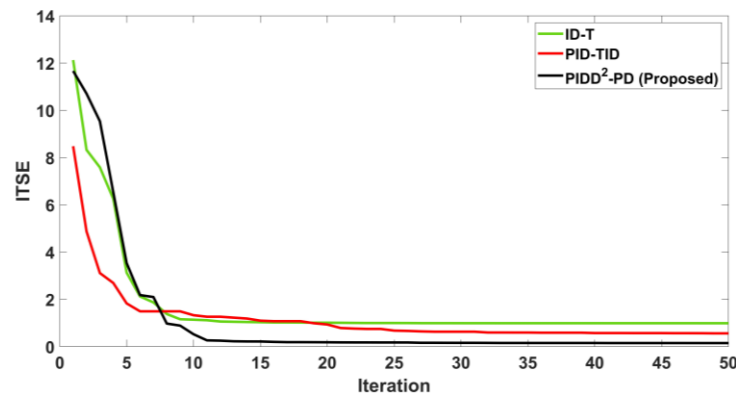


Figure 17. The convergence curve of the three controllers in Scenario (III).

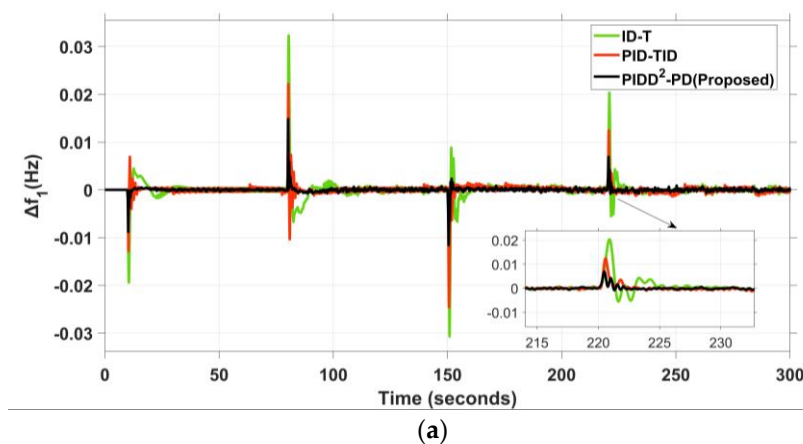


Figure 18. Cont.

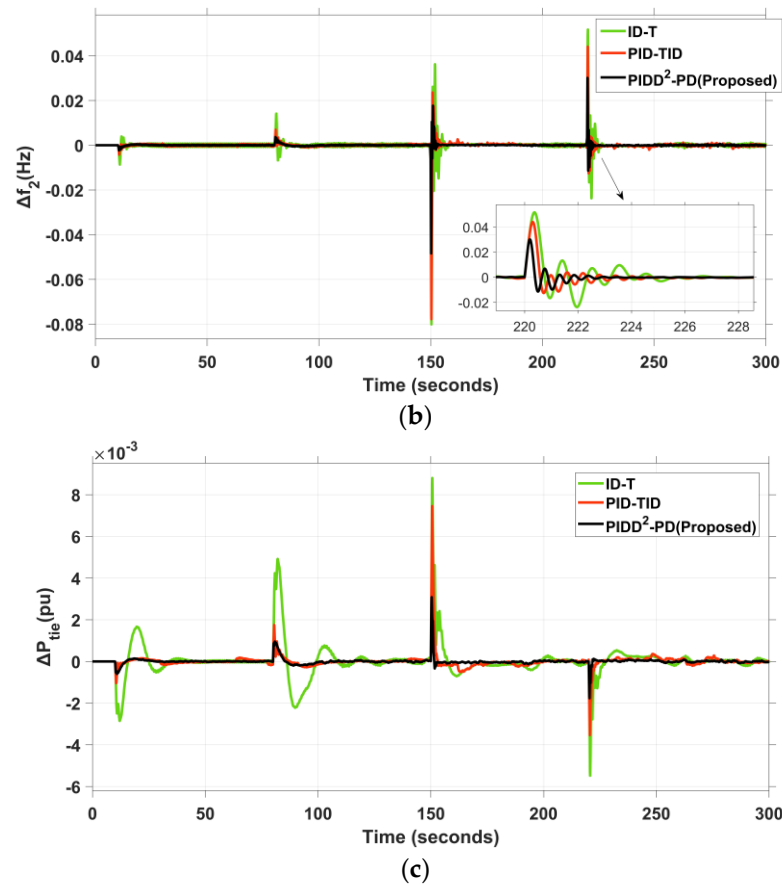


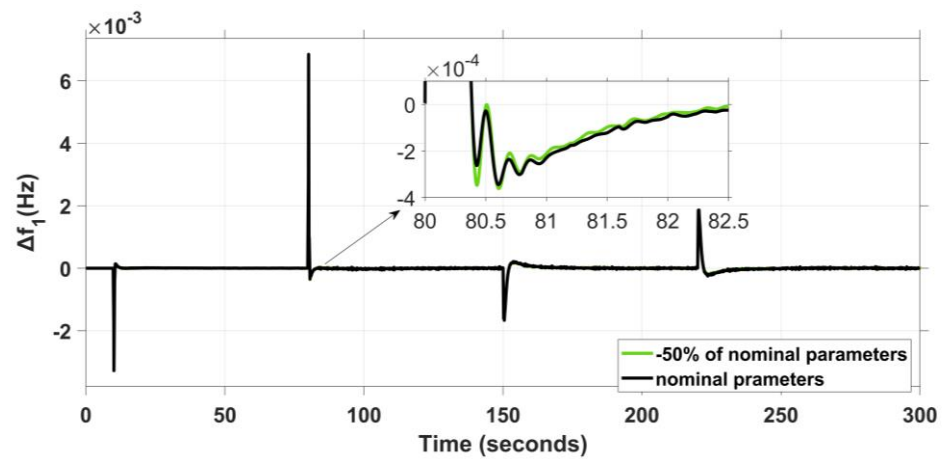
Figure 18. Dynamic power system response under Scenario III: (a) ΔF_1 , (b) ΔF_2 , and (c) ΔP_{tie} .

5.2.4. Scenario IV: Performance Evaluation for RESs and Changes in System Parameters

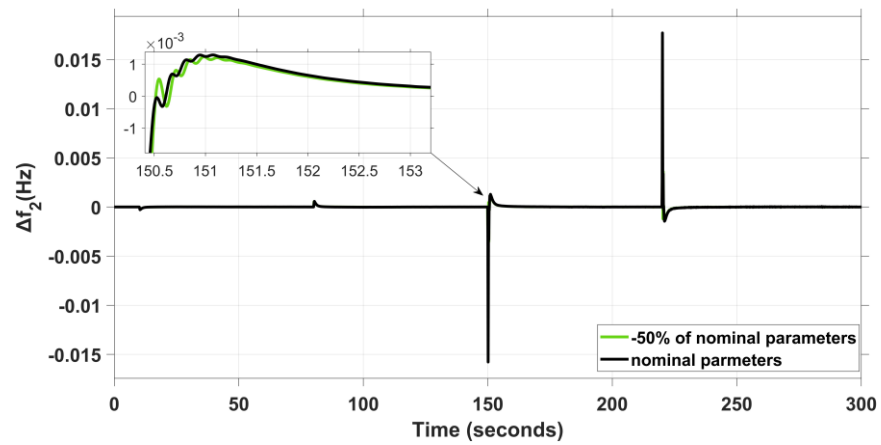
This scenario comprises the PIDD²-PD performance being investigated when system parameters, such as T_{sg} , T_t , T_{gh} , X_g , and Y_g , are changed by 50%. Step load penetration occurred in the first area at 10 s and the second area at 150 s, with values of 0.01 p.u and 0.03 p.u, respectively. The PV solar system and wind turbine are linked at 80 s and 220 s, respectively. Table 10 shows the settings of the suggested PIDD²-PD controller that are employed in this scenario. Table 14 shows the dynamic performance of the power system. Figures 19 and 20 clarify the frequency fluctuation of both areas of the power system network studied and flow power in the tie-line power when changing system settings by 50%. It can be concluded that changes of 50% in system settings, as well as step load penetration, applied to both areas, have a negligible effect on the functioning of the PIDD²-PD controller.

Table 14. Dynamic system response under effect Scenario IV.

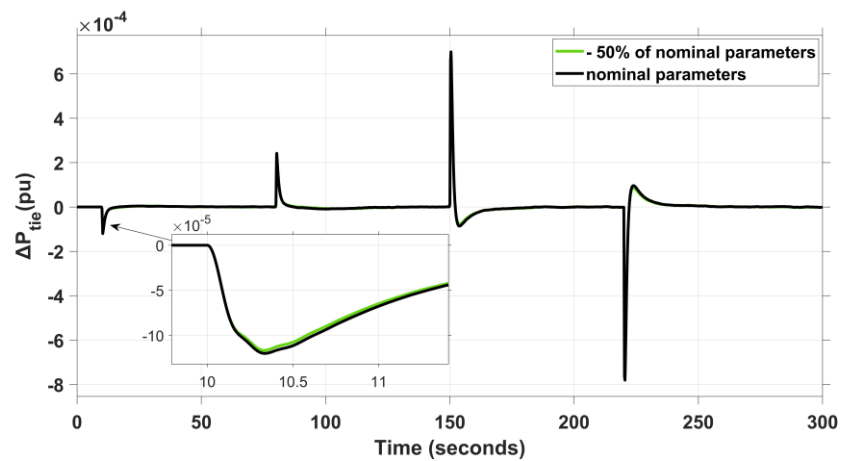
Controller	ΔF_1 (Hz)		ΔF_2 (Hz)		ΔP_{tie} (p.u)		ITSE
	Max. OS	Max. US	Max. OS	Max. US	Max. OS	Max. US	
PIDD ² -PD (suggested)	0.0068	0.0033	0.0177	0.0158	0.00070	0.00078	0.0167
PIDD ² -PD (suggested) with +50%	0.0068	0.0033	0.0178	0.0159	0.00072	0.00081	0.0172
PIDD ² -PD (suggested) with −50%	0.0068	0.0033	0.0176	0.0157	0.00065	0.00074	0.01583



(a)



(b)



(c)

Figure 19. Dynamic power system response under Scenario IV with a -50 change in the system settings: (a) Δf_1 , (b) Δf_2 , and (c) ΔP_{tie} .

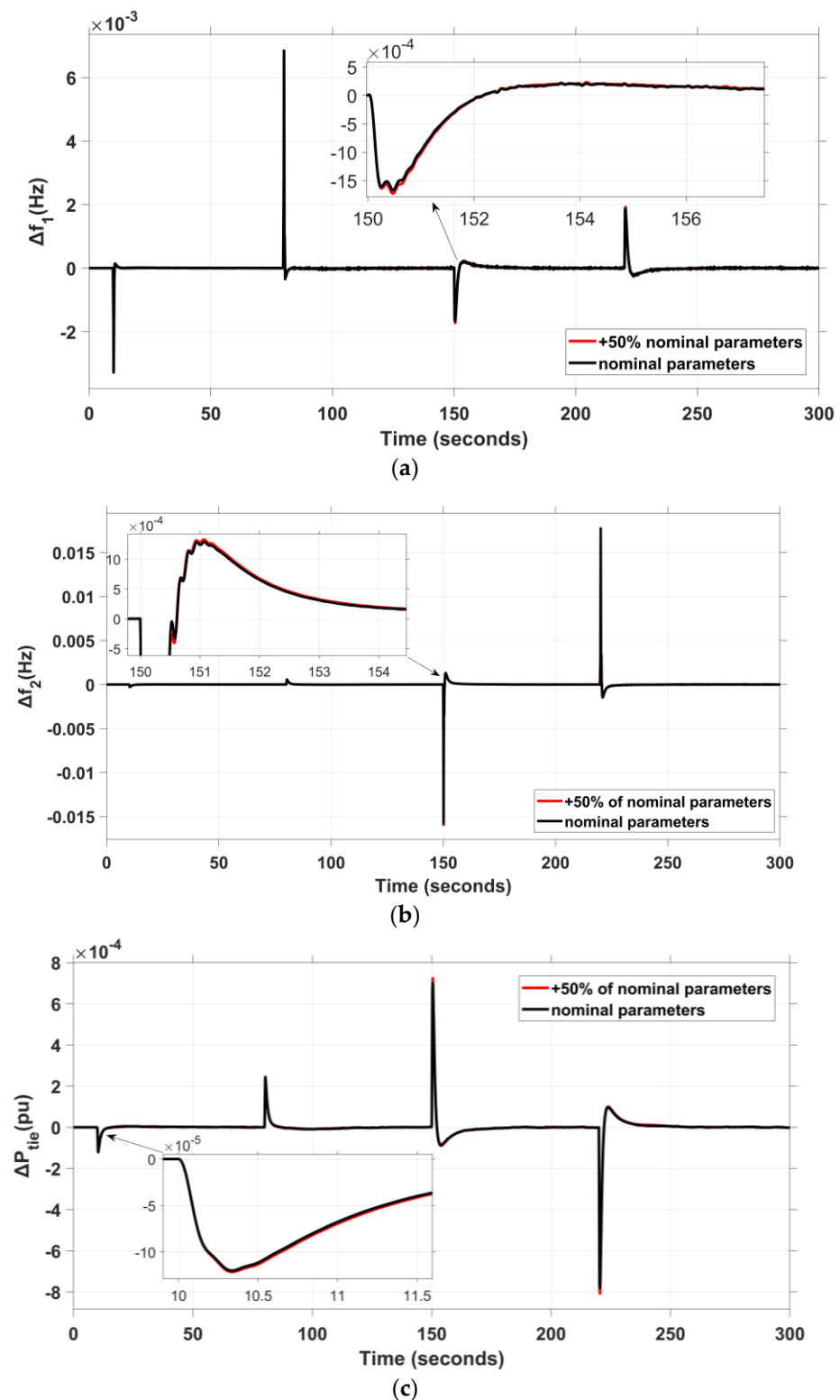


Figure 20. Dynamic power system response under Scenario IV with a +50 change in the system settings: (a) Δf_1 , (b) Δf_2 , and (c) ΔP_{tie} .

6. Conclusions

In this paper, a new controller structure known as a combined PIDD²-PD controller is developed for improving the frequency stability in the power system network understudied. In a two-area hybrid power system, each area consists of multiple conventional power stations and renewable energy sources. The suggested controller is implemented with

WOA, ChOA, and WHO algorithms. The WHO algorithm provides better performance, with a fast response. The effectiveness of the PIDD²-PD based on the WHO controller was compared to the PID-TID and ID-T controllers based on the WHO and ID-T controllers optimized for the AOA algorithm. A variety of different scenarios have been proposed to study the effectiveness of performance for the combined PIDD²-PD controller in addressing the issue of the two areas—load frequency control—by using different load patterns, RES disturbances, communication time delay, and system settings variations. From the above, it can be concluded the suggested controller achieves outstanding results in resolving all obstacles, increasing system stability, and enhancing the frequency dynamic response of the power system network. The PIDD²-PD controller has supremacy over the other controllers' performance. The suggested PIDD²-PD controller structure has been shown to be an excellent solution to the LFC issue.

Author Contributions: Conceptualization, M.K., M.R. and K.M.A.; Methodology, M.R., K.M.A. and N.H.A.; validation, M.K., M.R., K.M.A. and N.H.A.; formal analysis, M.K. and M.R.; investigation, K.M.A. and N.H.A.; resources, M.R., K.M.A., N.H.A.; writing—original draft preparation, M.K., M.R. and K.M.A.; writing—review and editing, K.M.A. and N.H.A.; visualization, M.R. and K.M.A. All authors have read and agreed to the published version of the manuscript.

Funding: This research received no external funding.

Institutional Review Board Statement: Not applicable.

Informed Consent Statement: Not applicable.

Data Availability Statement: Not applicable.

Conflicts of Interest: The authors declare no conflict of interest.

Nomenclature

AOA	Archimedes Optimization Algorithm
A_T	The rotor swept area (m^2)
B_1, B_2	Frequency bias coefficients
ChOA	Chimp Optimization Algorithm
C_p	The power coefficient of the rotor blades
CTD	Communication time delay
FF	Fitness function
FO	Fractional order
FOC	FO calculus
FOPID	Fractional order proportional derivative
GDB	Governor dead band
GRC	Generation rate constraint, % (p.u)
H	Total number of groups
ID-T	Integral derivative—tilted
I-PD	Integral-proportional derivative
it	Iteration
I-TD	Integral-tilted derivative
ITSE	Integral time squared error
kd	Derivative gain of PD
KD, KDD	Derivative gains of PIDD ²
KI	Integral gain of PIDD ²
KP	Proportional gain of PIDD ²
kp	The proportional gain of PD
LFC	Load frequency control
maxit	Maximum number of iterations
Max.OS	Maximum overshoot
MSLD	Multi-step load disturbances

Max.US	Maximum undershoot
N_d, N_{dd}	Filters' coefficients of the PIDD ²
nf	Filters' coefficients of the PD
PD	Proportional derivative
PID	Proportional integral derivative
PIDD ²	Proportional integral derivative—second derivative
PV	Photovoltaics
Q	Population size
RESs	Renewable energy sources
RLD	Random load disturbances
r_T	The rotor radius
SLD	Step load disturbances
SR	Number of stallions in the population
Set-Time	Settling time
TDC	Transient droop compensation
TID	Tilted integral derivative
T_s	Simulation time
V_W	The rated wind speed (m/s)
WHO	Wild Horse Optimization
WOA	Whale Optimization Algorithm
Z	Randomly selected adaptive mechanism
β	The pitch angle
ΔF_1	The frequency deviation in Area 1 (Hz)
ΔF_2	The frequency deviation in Area 2 (Hz)
ΔP_{tie}	The tie-line power deviation (p.u)
λ	The tip-speed ratio (TSR)
λ_I	The intermittent TSR
ρ	Air density (Kg/m ³)

References

- Magdy, G.; Mohamed, E.A.; Shabib, G.; Elbaset, A.A.; Mitani, Y. Microgrid dynamic security considering high penetration of renewable energy. *Prot. Control. Mod. Power Syst.* **2018**, *3*, 23. [\[CrossRef\]](#)
- Yang, Z.; Ghadamyari, M.; Khorramdel, H.; Alizadeh, S.M.S.; Pirouzi, S.; Milani, M.; Banihashemi, F.; Ghadimi, N. Robust multi-objective optimal design of islanded hybrid system with renewable and diesel sources/stationary and mobile energy storage systems. *Renew. Sustain. Energy Rev.* **2021**, *148*, 111295. [\[CrossRef\]](#)
- Dehghani, M.; Ghiasi, M.; Niknam, T.; Kavousi-Fard, A.; Shasadeghi, M.; Ghadimi, N.; Taghizadeh-Hesary, F. Blockchain-Based Securing of Data Exchange in a Power Transmission System Considering Congestion Management and Social Welfare. *Sustainability* **2021**, *13*, 90. [\[CrossRef\]](#)
- Magdy, G.; Shabib, G.; Elbaset, A.A.; Mitani, Y. Optimized coordinated control of LFC and SMES to enhance frequency stability of a real multi-source power system considering high renewable energy penetration. *Prot. Control. Mod. Power Syst.* **2018**, *3*, 39. [\[CrossRef\]](#)
- Khamies, M.; Magdy, G.; Kamel, S.; Khan, B. Optimal Model Predictive and Linear Quadratic Gaussian Control for Frequency Stability of Power Systems Considering Wind Energy. *IEEE Access* **2021**, *9*, 116453–116474. [\[CrossRef\]](#)
- Jagatheesan, K.; Anand, B.; Dey, N.; Ashour, A.S.; Balas, V.E. Load Frequency Control of Hydro-Hydro System with Fuzzy Logic Controller Considering Non-linearity. In *Recent Developments and the New Direction in Soft-Computing Foundations and Applications*; Springer: Cham, Switzerland, 2018; pp. 307–318.
- Nguyen, G.N.; Jagatheesan, K.; Ashour, A.S.; Anand, B.; Dey, N. Ant Colony Optimization Based Load Frequency Control of Multi-area Interconnected Thermal Power System with Governor Dead-Band Nonlinearity. In *Smart Trends in Systems, Security and Sustainability*; Springer: Singapore, 2018; pp. 157–167.
- Dritsas, L.; Kontouras, E.; Vlahakis, E.; Kitsios, I.; Halikias, G.; Tzes, A. Modelling issues and aggressive robust load frequency control of interconnected electric power systems. *Int. J. Control* **2022**, *95*, 753–767. [\[CrossRef\]](#)
- Tasnin, W.; Saikia, L.C.; Raju, M. Deregulated AGC of multi-area system incorporating dish-Stirling solar thermal and geothermal power plants using fractional order cascade controller. *Int. J. Electr. Power Energy Syst.* **2018**, *101*, 60–74. [\[CrossRef\]](#)
- Sharma, M.; Dhundhara, S.; Arya, Y.; Prakash, S. Frequency excursion mitigation strategy using a novel COA optimised fuzzy controller in wind integrated power systems. *IET Renew. Power Gener.* **2020**, *14*, 4071–4085. [\[CrossRef\]](#)
- Nandi, M.; Shiva, C.K.; Mukherjee, V. Moth-Flame Algorithm for TCSC- and SMES-Based Controller Design in Automatic Generation Control of a Two-Area Multi-unit Hydro-power System. *Iran. J. Sci. Technol.* **2020**, *44*, 1173–1196. [\[CrossRef\]](#)
- Jagatheesan, K.; Baskaran, A.; Dey, N.; Ashour, A.S.; Balas, V.E. Load frequency control of multi-area interconnected thermal power system: Artificial intelligence-based approach. *Int. J. Autom. Control* **2018**, *12*, 126–152. [\[CrossRef\]](#)

13. Eltamaly, A.M.; Zaki Diab, A.A.; Abo-Khalil, A.G. Robust Control Based on H_∞ and Linear Quadratic Gaussian of Load Frequency Control of Power Systems Integrated with Wind Energy System. In *Control and Operation of Grid-Connected Wind Energy Systems*; Springer: Cham, Switzerland, 2021; pp. 73–86.
14. Habib, D. Optimal Control of PID-FUZZY based on Gravitational Search Algorithm for Load Frequency Control. *Int. J. Eng. Res.* **2019**, *8*, 50013–50022.
15. Yakout, A.H.; Kotb, H.; Hasanien, H.M.; Aboras, K.M. Optimal Fuzzy PIDF Load Frequency Controller for Hybrid Microgrid System Using Marine Predator Algorithm. *IEEE Access* **2021**, *9*, 54220–54232. [[CrossRef](#)]
16. Magdy, G.; Mohamed, E.A.; Shabib, G.; Elbaset, A.A.; Mitani, Y. SMES based a new PID controller for frequency stability of a real hybrid power system considering high wind power penetration. *IET Renew. Power Gener.* **2018**, *12*, 1304–1313. [[CrossRef](#)]
17. Sharma, J.; Hote, Y.V.; Prasad, R. Robust PID Load Frequency Controller Design with Specific Gain and Phase Margin for Multi-area Power Systems. *IFAC-Pap.* **2018**, *51*, 627–632. [[CrossRef](#)]
18. Topno, P.N.; Chanana, S. Differential evolution algorithm based tilt integral derivative control for LFC problem of an interconnected hydro-thermal power system. *J. Vib. Control* **2017**, *24*, 3952–3973. [[CrossRef](#)]
19. Khokhar, B.; Dahiya, S.; Parmar, K.P.S. Load Frequency Control of a Multi-Microgrid System Incorporating Electric Vehicles. *Electr. Power Compon. Syst.* **2021**, *49*, 867–883. [[CrossRef](#)]
20. Elmelegi, A.; Mohamed, E.A.; Aly, M.; Ahmed, E.M.; Mohamed, A.A.A.; Elbaksawi, O. Optimized Tilt Fractional Order Cooperative Controllers for Preserving Frequency Stability in Renewable Energy-Based Power Systems. *IEEE Access* **2021**, *9*, 8261–8277. [[CrossRef](#)]
21. Morsali, J.; Zare, K.; Tarafdar Hagh, M. Comparative performance evaluation of fractional order controllers in LFC of two-area diverse-unit power system with considering GDB and GRC effects. *J. Electr. Syst. Inf. Technol.* **2018**, *5*, 708–722. [[CrossRef](#)]
22. Mohamed, E.A.; Ahmed, E.M.; Elmelegi, A.; Aly, M.; Elbaksawi, O.; Mohamed, A.A.A. An Optimized Hybrid Fractional Order Controller for Frequency Regulation in Multi-Area Power Systems. *IEEE Access* **2020**, *8*, 213899–213915. [[CrossRef](#)]
23. Ali, M.; Kotb, H.; Aboras, K.M.; Abbasy, N.H. Design of Cascaded PI-Fractional Order PID Controller for Improving the Frequency Response of Hybrid Microgrid System Using Gorilla Troops Optimizer. *IEEE Access* **2021**, *9*, 150715–150732. [[CrossRef](#)]
24. Prakash, A.; Murali, S.; Shankar, R.; Bhushan, R. HVDC tie-link modeling for restructured AGC using a novel fractional order cascade controller. *Electr. Power Syst. Res.* **2019**, *170*, 244–258. [[CrossRef](#)]
25. Saha, A.; Saikia, L.C. Load frequency control of a wind-thermal-split shaft gas turbine-based restructured power system integrating FACTS and energy storage devices. *Int. Trans. Electr. Energy Syst.* **2019**, *29*, e2756. [[CrossRef](#)]
26. Mohamed, T.H.; Shabib, G.; Abdelhameed, E.H.; Khamies, M.; Qudaih, Y. Load Frequency Control in Single Area System Using Model Predictive Control and Linear Quadratic Gaussian Techniques. *Int. J. Electr. Energy* **2015**, *3*, 141–143. [[CrossRef](#)]
27. Elkasem, A.H.A.; Khamies, M.; Hassan, M.H.; Agwa, A.M.; Kamel, S. Optimal Design of TD-TI Controller for LFC Considering Renewables Penetration by an Improved Chaos Game Optimizer. *Fractal Fract.* **2022**, *6*, 220. [[CrossRef](#)]
28. Daraz, A.; Malik, S.A.; Mokhlis, H.; Haq, I.U.; Laghari, G.F.; Mansor, N.N. Fitness Dependent Optimizer-Based Automatic Generation Control of Multi-Source Interconnected Power System with Non-Linearities. *IEEE Access* **2020**, *8*, 100989–101003. [[CrossRef](#)]
29. Singh, K.; Amir, M.; Ahmad, F.; Khan, M.A. An Integral Tilt Derivative Control Strategy for Frequency Control in Multimicrogrid System. *IEEE Syst. J.* **2021**, *15*, 1477–1488. [[CrossRef](#)]
30. Kumari, S.; Shankar, G.; Das, B. Integral-Tilt-Derivative Controller Based Performance Evaluation of Load Frequency Control of Deregulated Power System. In *Modeling, Simulation and Optimization*; Springer: Singapore, 2021; pp. 189–200.
31. Ahmed, M.; Magdy, G.; Khamies, M.; Kamel, S. Modified TID controller for load frequency control of a two-area interconnected diverse-unit power system. *Int. J. Electr. Power Energy Syst.* **2022**, *135*, 107528. [[CrossRef](#)]
32. Pahadasingh, S. TLBO Based CC-PID-TID Controller for Load Frequency Control of Multi Area Power System. In Proceedings of the 2021 1st Odisha International Conference on Electrical Power Engineering, Communication and Computing Technology (ODICON), Bhubaneswar, India, 8–9 January 2021.
33. Paliwal, N.; Srivastava, L.; Pandit, M. Application of grey wolf optimization algorithm for load frequency control in multi-source single area power system. *Evol. Intell.* **2020**, *15*, 563–584. [[CrossRef](#)]
34. Revathi, D.; Mohan Kumar, G. Analysis of LFC in PV-thermal-thermal interconnected power system using fuzzy gain scheduling. *Int. Trans. Electr. Energy Syst.* **2020**, *30*, e12336. [[CrossRef](#)]
35. Jagatheesan, K.; Anand, B.; Dey, N.; Gaber, T.; Hassanien, A.E.; Kim, T.H. A Design of PI Controller using Stochastic Particle Swarm Optimization in Load Frequency Control of Thermal Power Systems. In Proceedings of the 2015 Fourth International Conference on Information Science and Industrial Applications (ISI), Busan, Korea, 20–22 September 2015.
36. Ah, G.H.; Li, Y.Y. Ant lion optimized hybrid intelligent PID-based sliding mode controller for frequency regulation of interconnected multi-area power systems. *Trans. Inst. Meas. Control* **2020**, *42*, 1594–1617. [[CrossRef](#)]
37. Patel, N.C.; Sahu, B.K.; Khamari, R.C. TLBO Designed 2-DOFPIDF Controller for LFC of Multi-area Multi-source Power System. In *Innovation in Electrical Power Engineering, Communication, and Computing Technology*; Springer: Singapore, 2022; pp. 269–282.
38. Aryan, P.; Ranjan, M.; Shankar, R. Deregulated LFC scheme using equilibrium optimized Type-2 fuzzy controller. In Proceedings of the International conference on Innovative Development and Engineering Applications, Gaya, India, 8–10 February 2021.

39. Khokhar, B.; Dahiya, S.S.; Singh Parmar, K.P. Atom search optimization based study of frequency deviation response of a hybrid power system. In Proceedings of the 2020 IEEE 9th Power India International Conference (PIICON), Murthal, India, 28 February–1 March 2020; pp. 1–5.
40. Naruei, I.; Keynia, F. Wild horse optimizer: A new meta-heuristic algorithm for solving engineering optimization problems. *Eng. Comput.* **2021**, *1*–32. [[CrossRef](#)]
41. Khishe, M.; Mosavi, M.R. Chimp optimization algorithm. *Expert Syst. Appl.* **2020**, *149*, 113338. [[CrossRef](#)]
42. Mirjalili, S.; Lewis, A. The Whale Optimization Algorithm. *Adv. Eng. Softw.* **2016**, *95*, 51–67. [[CrossRef](#)]
43. Parmar, K.P.S.; Majhi, S.; Kothari, D.P. LFC of an Interconnected Power System with Thyristor Controlled Phase Shifter in the Tie Line. *Int. J. Comput. Appl.* **2012**, *41*, 27–30.
44. Magdy, G.; Shabib, G.; Elbaset, A.A.; Kerdphol, T.; Qudaih, Y.; Mitani, Y. Decentralized optimal LFC for a real hybrid power system considering renewable energy sources. *J. Eng. Sci. Technol.* **2019**, *14*, 682–697.
45. Ali, M.; Kotb, H.; AboRas, M.K.; Abbasy, H.N. Frequency regulation of hybrid multi-area power system using wild horse optimizer based new combined Fuzzy Fractional-Order PI and TID controllers. *Alex. Eng. J.* **2022**, *61*, 12187–12210. [[CrossRef](#)]
46. Kalyan, C.N.S.; Suresh, C.V. PIDD controller for AGC of nonlinear system with PEV integration and AC-DC links. In Proceedings of the 2021 International Conference on Sustainable Energy and Future Electric Transportation (SEFET), Hyderabad, India, 21–23 January 2021.